

U-Pb zircon dating, Sr-Nd isotope and petrogenesis of Sarduiyeh granitoid in SE of the UDMA, Iran: implication for the source origin and magmatic evolution

Asma Nazarinia, Mohsen Mortazavi, Mohsen Arvin, Ruizhong Hu, Chenghai Zhao & Mohammad Poosti

To cite this article: Asma Nazarinia, Mohsen Mortazavi, Mohsen Arvin, Ruizhong Hu, Chenghai Zhao & Mohammad Poosti (2018): U-Pb zircon dating, Sr-Nd isotope and petrogenesis of Sarduiyeh granitoid in SE of the UDMA, Iran: implication for the source origin and magmatic evolution, International Geology Review, DOI: [10.1080/00206814.2018.1514668](https://doi.org/10.1080/00206814.2018.1514668)

To link to this article: <https://doi.org/10.1080/00206814.2018.1514668>

 View supplementary material 

 Published online: 17 Sep 2018.

 Submit your article to this journal 

 View Crossmark data 

U-Pb zircon dating, Sr-Nd isotope and petrogenesis of Sarduiyeh granitoid in SE of the UDMA, Iran: implication for the source origin and magmatic evolution

Asma Nazarinia^a, Mohsen Mortazavi^a, Mohsen Arvin^b, Ruizhong Hu^c, Chenghai Zhao^c and Mohammad Poosti^a

^aDepartment of Geology, Faculty of Sciences, University of Hormozgan, Bandar Abbas, Iran; ^bDepartment of Geology, Faculty of Sciences, Shahid Bahonar University of Kerman, Kerman, Iran; ^cState Key Laboratory of Ore Deposit Geochemistry, Institute of Geochemistry, Chinese Academy of Sciences, Guiyang, China

ABSTRACT

The Sarduiyeh granitoid (SG) is intruded in the southeastern part of the Dehaj-Sarduiyeh volcano-sedimentary belt in the southeastern end of the Urumieh-Dokhtar Magmatic Arc (UDMA) in Iran. The medium-to-coarse-grained granitoid unit, with granular texture consists mainly of diorite, tonalite, granodiorite and monzogranitic rocks. Mineralogically, these rocks consist mainly of plagioclase, K-feldspar, quartz, biotite and hornblende. The whole rock geochemical analyses indicates that the SG is calc-alkaline, I-type, metaluminous, enriched in large ion lithophile elements (LILE; such as K, Cs, Pb) and depleted in high field strength elements (HFSE; such as Ti, Nb, Ta, Zr). Chondrite normalized plot of SG rare earth elements (REE) show light rare earth element enrichments with ($La_N/Yb_N = 2.44-8.68$) and flat heavy rare earth element patterns with ($Gd_N/Yb_N = 1.02-1.36$). The rather high Y (*av.* 19.35 ppm), low Sr content (*av.* 293.76 ppm) and low Cr and Ni contents (*av.* 20.1 and 4.69 ppm, respectively) of the SG demonstrate its normal calc-alkaline and non-adakitic nature, the features of Jebal Barez-type granitoids. The geochemical characteristics and isotopic composition, low I_{Sr} (0.7046–0.7049) and positive $\epsilon^{147}Nd$ (+3.4 to +4.03) values, of the SG suggest that its parental magma formed as a result of partial melting from metabasic rocks of lower crust in a subduction-related arc setting. Fractionation of an assemblage dominated by plagioclase, K-feldspar, amphibole and magnetite may have been responsible for the evolution of the SG magma. U-Pb zircon geochronology gives an age of 27.95 ± 0.27 Ma for the SG, suggesting that the final collision between the Arabian plate and Central Iranian microcontinent may have happened in the Late Oligocene.

ARTICLE HISTORY

Received 26 February 2018
Accepted 19 August 2018

KEYWORDS

Sarduiyeh granitoid; UDMA; Dehaj-Sarduiyeh volcano-sedimentary belt; U-Pb dating; fractionation; Iran

1. Introduction

The subduction of Neo-Tethys oceanic crust under the Central Iranian microcontinent during Late Mesozoic-Early Tertiary led to the collision of Arabian plate with Eurasia and subsequent formation of the Zagros Orogeny Belt (ZOB) in Iran (Dercourt *et al.* 1986; Stampfli and Borel 2002; Arvin *et al.* 2007; Shahbazi *et al.* 2010; Agard *et al.* 2011; Azizi *et al.* 2011; Mazhari *et al.* 2011; Mouthereau *et al.* 2012). The timing of closure of the Neo-Tethys is speculative and it is reported during (a) Late Cretaceous (Berberian and King 1981; Alavi 1994, 2004; Mohajjel and Fergusson 2000), (b) Late Eocene to Oligocene (e.g. Dargahi *et al.* 2010; Verdel *et al.* 2011; Chiu *et al.* 2013; Shafaii Moghadam *et al.* 2015), (c) Miocene (Berberian and Berberian 1981; Verdel *et al.* 2011) or (d) Pliocene (Stöcklin 1968).

The ZOB trends NW-SE for about 2000 km from the Turkish-Iranian border to the Makran in southeastern Iran (Mohajjel *et al.* 2003) and includes three sub-parallel

tectono-stratigraphic segments (Agard *et al.* 2005; Takin 1972; Alavi 1994, 2004; Bushara 1995; Mohajjel *et al.* 2003). The three parts are shown in Figure 1, as the Zagros Fold-Thrust Belt (ZFTB) (Stöcklin 1968; Berberian and King 1981; Mohajjel and Fergusson 2000), the Sanandaj-Sirjan Zone (SSZ) and Urumieh-Dokhtar Magmatic Arc (UDMA). The main Zagros thrust line separates the SSZ from the ZFTB to the southeast, whereas to the northeast the boundary of the SSZ with the UDMA is characterized by a series of basins that are interpreted to be forearc depressions, laterally equivalent to the Makran belt (Alavi 1994; Glennie 2000). The ZFTB is easily recognized by well-developed, large NW-SE trending anticlines and synclines which were formed predominantly by flexural slip folding mechanism (Colman Sadd 1978; Bahroudi and Talbot 2003). The SSZ is characterized by Proterozoic-Mesozoic metamorphic rocks such as schists, gneisses, amphibolites, metacarbonates, abundant deformed and undeformed plutons, and widespread Mesozoic volcanic rocks (Stöcklin 1968). The UDMA is composed of calc-

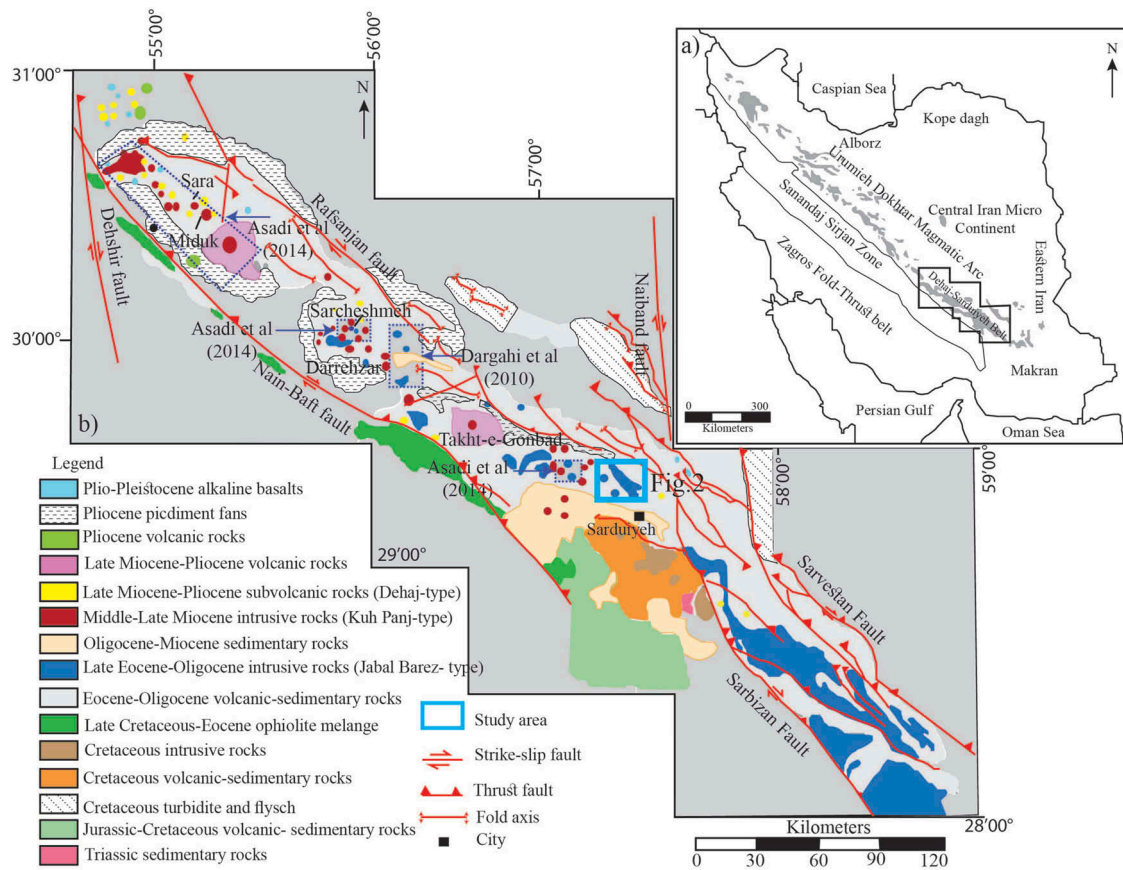


Figure 1. (a) Simplified map of major structural units of Iran (after Alavi 1996) and location of the Dehaj-Sarduiyeh volcano-sedimentary belt in the Urumieh-Dokhtar magmatic arc (compiled from Dimitrijevic 1973; Saric and Mijalkovic 1973; Stöcklin and Nabavi 1973; Emami *et al.* 1993). (b) Simplified geological map of the Dehaj-Sarduiyeh volcano-sedimentary belt and location of Sarduiyeh granitoid (Dimitrijevic 1973; Shafiei *et al.* 2009).

alkaline, locally tholeiitic and K-rich alkaline intrusive and extrusive rocks (Ahmad and Posht Kahi 1993; Golonka 2004; Omrani *et al.* 2008). The oldest rocks in the UDMA are calc-alkaline intrusive rocks, which cut across the Upper Jurassic formations and are overlain unconformably by Lower Cretaceous fossiliferous limestone. The youngest rocks in the UDMA consist of Pliocene to Quaternary lava flows and pyroclastic that show alkaline and calc-alkaline affinities (Berberian and Berberian 1981). Most of granitoid magmas in the UDMA are inferred to have been formed in a subduction related tectonic setting (Berberian and King 1981). Although the tectonic setting of the granitoid magmas in a subduction zone is well documented in UDMA (e.g. Agard *et al.* 2005; Berberian and King 1981), the origin of the parental magmas and the processes that led to their formation remain controversial (Omrani *et al.* 2008; Yaganehfar *et al.* 2013; Kananian *et al.* 2014).

The southeastern part of UDMA in the Kerman province is known as Dehaj-Sarduiyeh volcano-sedimentary belt (Dimitrijevic 1973) or Kerman Cenozoic Magmatic Arc (KCMA); (Hassanzadeh 1993; Shahabpour 2005;

Shafiei 2008); (Figure 1(a)). Generally, the KCMA contains two different types of intrusions (Dimitrijevic 1973; Shafiei 2008): (1) the Jebal Barez-type (non-adakitic) and (2) Kuh Panj-type intrusions (adakite-like). Dargahi *et al.* (2010) studied three granitoid stocks in southwest of the Dehaj-Sarduiyeh volcano-sedimentary belt (Figure 1 (b)) and suggested that they are probably derived from partial melting of an enriched lithospheric mantle source that was modified by slab-derived components from an earlier subducting event. Asadi *et al.* (2014) studied some granitoid intrusions in the Dehaj-Sarduiyeh volcano-sedimentary belt and suggested that they either formed by partial melting of a garnet-free basaltic amphibolite (Jebal-Barez type) or by melting of the lower continental crust in the presence of a garnet source (Kuh-Panj type). As a part of the Dehaj-Sarduiyeh volcano-sedimentary belt a batholith and two stock size granitoid outcrops (hereafter referred to as Sarduiyeh granitoid (SG) were chosen in the NW of city of Sarduiyeh for this study (Figure 1(b)). We hereby report the whole rock geochemical composition, mineral chemistry, U-Pb age dating and Sr-Nd isotope

ratios of the SG for the first time. Furthermore, where the data was available, a comparison has been made between the SG and similar granitoid rock types in the KCMA. The major goals of this study are to understand: the geochemical composition, of the SG, characteristics of its melting source, the age and the effective mechanisms that were involved in the petrogenesis of the SG. We hope this will eventually shed some light on the magmatic evolution in southeastern part of the UDMA.

2. Geology of study area

Tertiary magmatic activities in the Dehaj-Sarduiyeh volcano-sedimentary belt (Figure 1(a)) led to the formation of two types of granitoid intrusions: Jebal Barez type and Kuh Panj type (Dimitrijevic 1973; Hassanzadeh 1993; Shahabpour 2005; Shafiei 2008). The Jebal Barez intrusions occur as batholith and stock-size bodies and show granular texture (Dimitrijevic 1973; Shafiei 2008). In contrast, Kuh Panj granitoids (adakite-like) mainly developed as stocks with porphyritic texture (Dimitrijevic 1973; Dargahi 2007). The intrusions show a linear trend from Dehaj area in the NW to Jebal Barez area in the SE (Figure 1(b)). Field relationships (Dimitrijevic 1973) together with available radiometric data (Conrad *et al.* 1977; McInnes *et al.* 2003) indicated that intrusive activities in Dehaj-Sarduiyeh volcano-sedimentary belt began in the Middle Eocene to Oligocene with the formation of Jebal Barez type intrusions and followed by Kuh-Panj hypabyssal-type granitoid intrusions during Middle to

Late Miocene-Pliocene (Berberian *et al.* 1982; Mohajjel *et al.* 2003; Dargahi 2007). Several studies show that the Jebal Barez and Kuh Panj types vary in age from 16.9 ± 0.2 to 29.7 ± 0.3 Ma (Conrad *et al.* 1977; Ghorashi Zadeh 1978; Hassanzadeh 1993; McInnes *et al.* 2003; Aghazadeh *et al.* 2015) and from 4.9 ± 0.4 to 13.3 ± 1.1 Ma, respectively (Ghorashi Zadeh 1978; Shahabpour and Kramers 1987; Hassanzadeh 1993; McInnes *et al.* 2003, 2005). Geological data and radiometric dating suggest that the Kuh Panj-type granitoids are associated with extensive porphyry copper mineralization in the Kerman province, SE of Iran, also known as Kerman porphyry copper belt (KPCB; Ghorashi Zadeh 1978; Shahabpour and Kramers 1987; Hassanzadeh 1993; McInnes *et al.* 2003; Shafiei 2008). No porphyry copper deposits have been reported in the Jebal Barez-type granitoids (Conrad *et al.* 1977; Hassanzadeh 1993; McInnes *et al.* 2003). The SG intruded Eocene volcanic rocks of Dehaj-Sarduiyeh volcano-sedimentary belt which consists mainly of andesite, andesite-basalt and scarce basalt with pyroclastic (Dimitrijevic 1973; Figure 2).

The SG is in sharp contact with its host Eocene volcanic rocks (Figure 3(a)) and is exposed along the several NW-SE trending fault lines (Figure 1(b)). These structural lineaments may have controlled the emplacement of SG, as it has been suggested by many workers (Leake 1990; Cobbing 1996). The SG with intermediate to felsic composition, consist of diorite, tonalite, granodiorite and monzogranite. The contacts between different rock types are gradual that suggest a petrogenetic

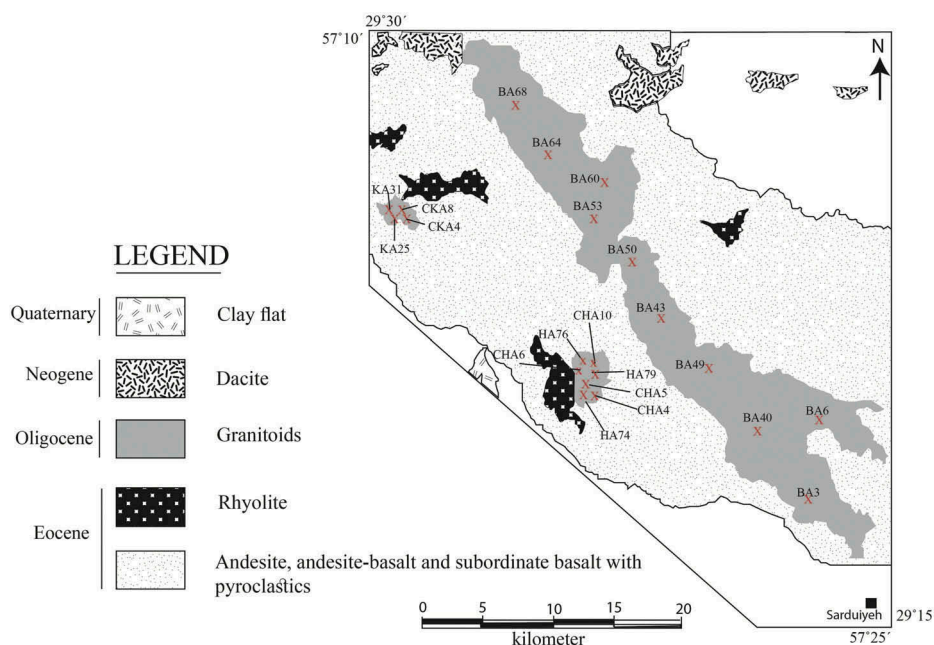


Figure 2. Simplified geological map of the study area (modified after Dimitrijevic 1973) and approximate location of the samples analysed.

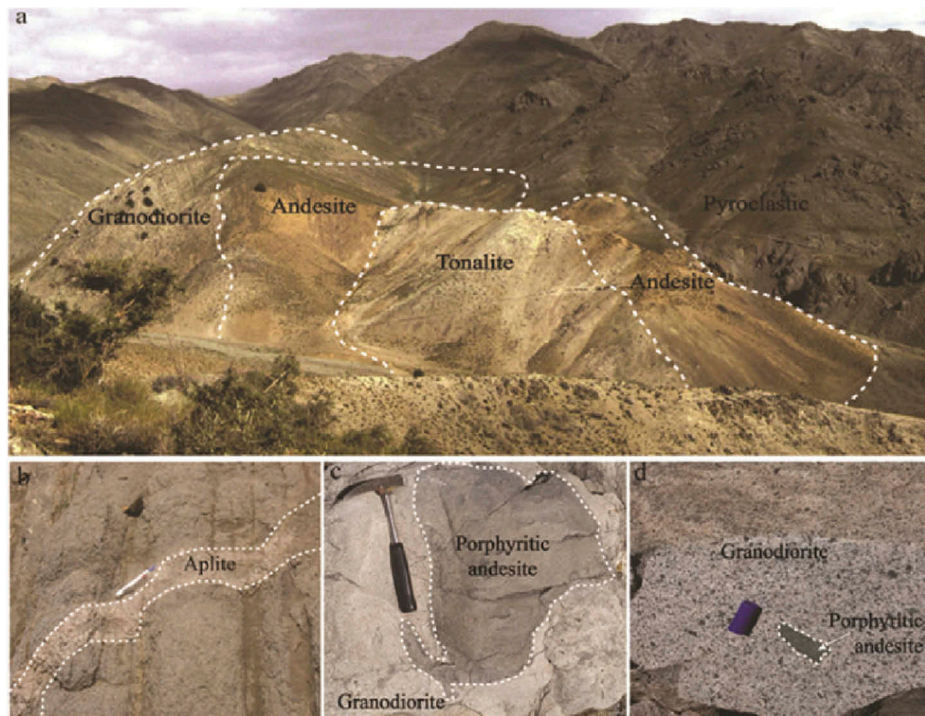


Figure 3. (a) Field photographs of intrusive and volcanic rocks in the study area (b) Aplitic dyke cutting through the granodiorite rock. (c,d) Xenoliths in the granodiorite.

link between them. Aplitic dykes (ca. 20–70 cm in width) with fine-grained aplitic texture are common (Figure 3(b)). A few circular or elliptical to angular xenoliths are scattered along the margins of the pluton and are very fine-grained in comparison to the granitoid. The xenoliths mainly consist of hornfelsic fragments of the pre-existing Eocene porphyritic andesite, ranging in size from 1 to 35 cm (Figure 3(c,d)).

3. Analytical methods

The total of 130 samples was collected from the SG outcrops and drill cores. Based on detail petrographic examination, twenty samples were selected from fresh to mildly altered rocks for whole rocks analyses.

Chemical composition analyses on plagioclase, k-feldspar and amphibole of 7 representative samples from SG were conducted by using wavelength-dispersive X-ray approach on an EPMA-1600 electron probe at the SKLODG (Supplementary Tables 1 and 2). Standard operating conditions include 25 kv for accelerating voltage, 10 nA for specimen current and 10 μm for beam diameter. SPI mineral standards (USA) were used for calibration.

Thirty Zircons were separated from sample BA40 using standard crushing, heavy liquid, and isodynamic separation techniques at the Geological Survey of Iran. Cathodoluminescence (CL) images were acquired to

characterize internal structures of zircons in order to choose appropriate sites for U-Pb analysis.

The dating of the granodiorite was undertaken by using ELAN DRC-e ICP-MS equipped with 193 nm Excimer laser at the SKLODG. The detailed operating conditions for the laser ablation system and the ICP-MS instrument and data reduction are described by Liu *et al.* (2008) and Liu *et al.* (2010a), Liu *et al.* (2010b). Off-line selection and integration of background and analytic signals, and mass bias calibrations were performed using ICPMS DataCal (Liu *et al.* 2008, 2010b). The U-Pb ratios were also calibrated by Zircon 91500. The results are shown in Supplementary Tables 3 and 4.

Major elements of whole rocks were measured using an Axios PW4400 X-ray fluorescence spectrometer (XRF) on fused lithium-tetraborate glass beads at the ALS Chemex Co., Ltd, Guangzhou, China. Trace elements were analysed by PerkinElmer Sciex ELANDRC-e ICP-MS at the State Key Laboratory of Ore Deposit Geochemistry (SKLODG). 50 mg powdered samples were dissolved in high pressure Teflon bombs using Hf and HNO_3 acids mixture at about 190°C for 2 days, with Rh as an internal standard to monitor signal drift during counting. Detailed analytical methods were introduced by Qi *et al.* (2000). Quality control limits for reference materials and duplicate analyses are established according to the precision and accuracy requirements of the particular method. The sensitivity of the

instrument was adjusted to more than 30,000 cps for 1 ng/ml of ^{115}In , in order to achieve the desired detection limits. Results indicate an error less than 0.6% for major elements, except CaO (1.02%), MnO (5.88%) and P_2O_5 (4.21%), and <10% for trace elements except Sc (11.3%). The results of analyses together with detection limits and standard sample (GBW07110 for XRF, AGV-2 for ICP-MS) for each element are shown in Supplementary Table 5. Furthermore, for measuring the loss on ignition (LOI) a 1.0 g of prepared sample is placed for one hour in an oven at 1000°C , then cooled and weighed. The LOI is calculated by weight difference.

Sr and Nd isotopes ratios were determined for 11 selected samples at the SKLODG (Supplementary Table 6). Approximately 100–1500 mg of whole-rock powder was completely decomposed in a mixture of HF-HClO_4 for Sr-Nd isotopic analysis. Sr-Nd were separated on quartz columns by conventional ion exchange chromatography with a 5-ml resin bed of AG 50W-X12 (200–400 mesh). Nd and Sm were separated from other rare earth elements on quartz columns using 1.7-ml Teflon powder coated with HDEHP, di (2-ethylhexyl) orthophosphoric acid, as cation exchange medium. Sr was loaded with a Ta-Hf activator on pre-conditioned W filaments and was measured in single-filament mode. Nd was loaded as phosphate on pre-conditioned Re filaments and measurements were performed in a Re

double filament configuration. The $^{87}\text{Sr}/^{86}\text{Sr}$ and $^{143}\text{Nd}/^{144}\text{Nd}$ ratios are normalized to $^{86}\text{Sr}/^{88}\text{Sr} = 0.1194$ and $^{146}\text{Nd}/^{144}\text{Nd} = 0.7219$, respectively. In the LRIG, repeated measurements of Ames metal and the NBS987 Sr standard during the 2004/2005 period gave mean values of 0.512149 ± 0.00002 ($n = 98$) for the $^{87}\text{Sr}/^{86}\text{Sr}$ ratio. Results of repeated Rb-Sr and Sm-Nd analyses on the standard BCR-1 (basalt powder) are given in Supplementary Table 6. The analyses were carried out at the SKLODG. The external precision refers to the 2σ uncertainty based on replicate measurements on these standard solutions over one year. Total procedural blanks were <300 pg for Sr and <50 pg for Nd.

4. Results

4.1. Petrography

Using modal analyses, the Sarduiyeh granitoid units are classified as, diorite, tonalite, granodiorite and monzogranite on the QAP diagram (Figure 4) with mainly medium to coarse grain and granular texture (Figure 5(a)). Mineralogically, these rocks consist mainly of plagioclase (20–62 vol.%), quartz (4–30 vol.%), K-feldspar (0–37 vol.%), biotite (2–12 vol.%) and hornblende (4–26 vol.%) (Figure 5(b)). Magnetite, titanite, apatite, zircon are found as accessory minerals. Secondary mineral phases are chlorite, calcite, sericite, epidote and kaolinite.

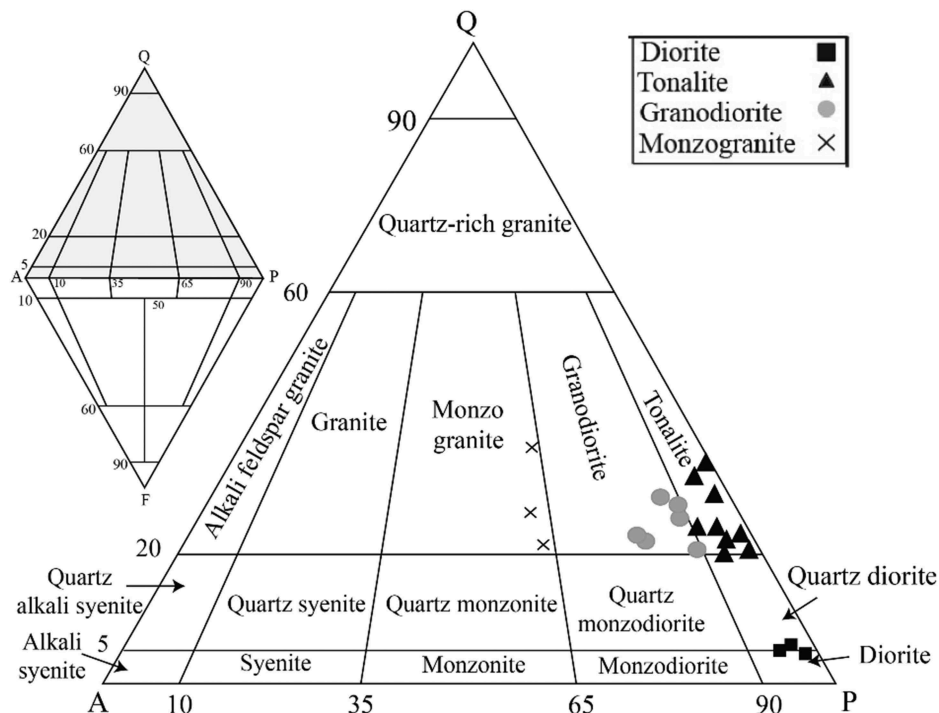


Figure 4. Q-A-P plot showing the relative proportions of quartz (Q), alkali feldspar (A), and plagioclase (P) for Sarduiyeh granitoid rocks (after Lemaitre *et al.* 2002).

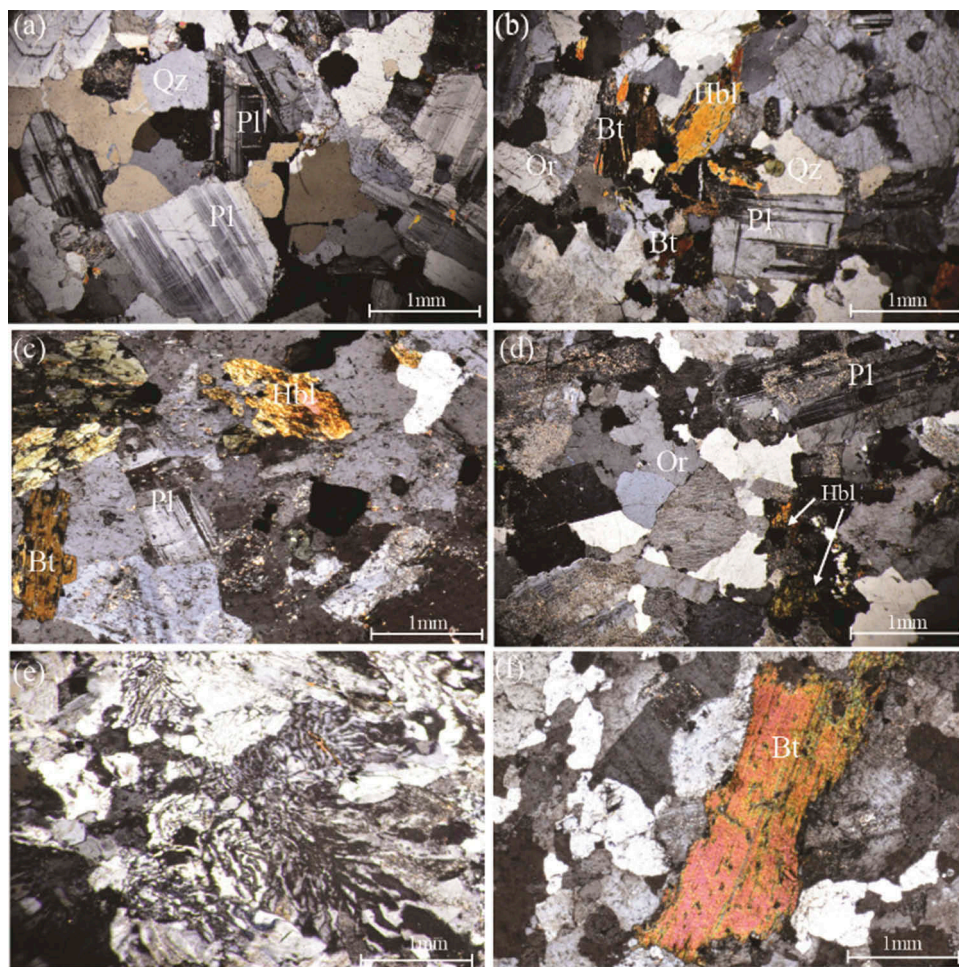


Figure 5. Crossed polarized light representative photomicrographs of the Sarduiyeh granitoid rocks. (a) Polysynthetic twinning in the plagioclase and granular texture. (b) Major mineral assemblages of plagioclase, quartz, orthoclase, hornblende and biotite. (c) Orthoclase showing perthitic texture. (d) Granophyre texture showing intergrowth of quartz and alkali feldspar. (e) Hornblende, plagioclase and biotite in granodiorite (f) Biotite altered to chlorite in monzogranite. Mineral abbreviations based on Whitney and Evans (2010): Qz, quartz; Pl, plagioclase; Or, Orthoclase; Hbl, hornblende; Bt, biotite; Opa, opaque.

Plagioclase occurs as euhedral to subhedral crystals (0.3–2.5 mm in size) with polysynthetic and Carlsbad-albite twinning. Sericitation is common in this mineral. K-feldspar mostly occurs as anhedral grains of orthoclase and often show Carlsbad twinning, alongside with perthitic texture (Figure 5(c)). Sericitation is common around the edges of the mineral. Fine to medium quartz grains grow in interstitial spaces between the other mineral and occasionally show intergrowths with K-feldspar to form a granophyre texture (Figure 5(d)). Hornblende commonly occurs as subhedral prismatic medium size crystals (Figure 5(e)) that in some samples has been altered to chlorite and epidote. Biotites (1–2.5 mm in size), form subhedral to anhedral crystals and it is locally altered in some samples to chlorite (Figure 5(f)). Apatite and zircon occur as very long needle-like crystals and euhedral to subhedral grains, respectively. These tiny accessory minerals are typically embedded in biotites and hornblendes. Opaque

minerals are common in the groundmass and as inclusions in hornblende. Most magnetite grains are euhedral, which points to their primary nature (Clarke 1992).

4.2. Mineral chemistry

Plagioclase, K-feldspar and amphibole crystals of representative SG samples were analysed for their compositions. All the feldspars and amphibole were analysed from core to the rim and no significant variations were detected in their compositions (Supplementary Tables 1 and 2). The plagioclases are mainly andesine and labradorite ($An_{29-54}Ab_{43-65}Or_{1-5}$) whereas the K-feldspars mainly plot in orthoclase field ($Or_{74-78} - Ab_{18-22}$) (Supplementary Table 1, Supplementary Figure 1(a,b)).

Amphibole as the most common mafic mineral in the SG show a limited compositional variation. The chemical compositions of the amphiboles (Supplementary Table 2) are plotted in the calcic group on BNa versus

BCa + BNa diagram (Leake *et al.* 1997; Supplementary Figure 2(a)). Based on the Mg/(Mg + Fe²⁺) versus TSi diagram, amphiboles are classified as magnesio-hornblende (Supplementary Figure 2(b)).

4.3. Zircon U-Pb age

The zircons occur as euhedral colourless grains. They are mostly elongated and have length/width ratios of 2 to >6 (Figure 6). This ratio is commonly believed to reflect crystallization velocity of zircon (Corfu *et al.* 2003). Stubby and equant forms of zircon are common in slowly cooled deep-seated intrusions, whereas needle-like and acicular zircons are more common in rapidly crystallized, porphyritic and sub-volcanic intrusions (Corfu *et al.* 2003). The lack of the needle-like and acicular zircon show a slowly cooled conditions. The uranium (35.30–172.02 ppm) and thorium (18.66–243.38 ppm) concentrations and high Th/U ratios (0.52–1.22) in zircons, show their magmatic origin (Belousova *et al.* 2002). In contrast, the metamorphic

zircons have Th/U < 0.1 (Vavra *et al.* 1996, 1999; Rubatto 2002). One of the most diagnostic features of magmatic zircon is its presence of well-developed growth zoning. In CL images of the zircon from the granodiorite sample number BA46 (Figure 6) the zircon grains show concentric oscillatory zoning which depict its magmatic origin.

Thirty zircons from granodiorite sample number BA46 were analysed by the U/Pb zircon method to determine the crystallization age (Supplementary Table 3). The data define a population on a concordia diagram with a weighted mean ²⁰⁶Pb/²³⁸U age of 27.95 ± 0.27 Ma (MSWD = 0.62) (Figure 7).

The REE compositions of the zircons are presented in Table 4. Chondrite normalized plot of rare earth elements show steeply increasing slope from LREE to HREE, which is characteristics of igneous zircon (Hoskin and Schaltegger 2003) and display a positive Ce anomaly (Ce/Ce* = 2.85–41.63) and negative Eu anomaly (Eu/Eu* = 0.007–0.364) (Supplementary Figure 3).

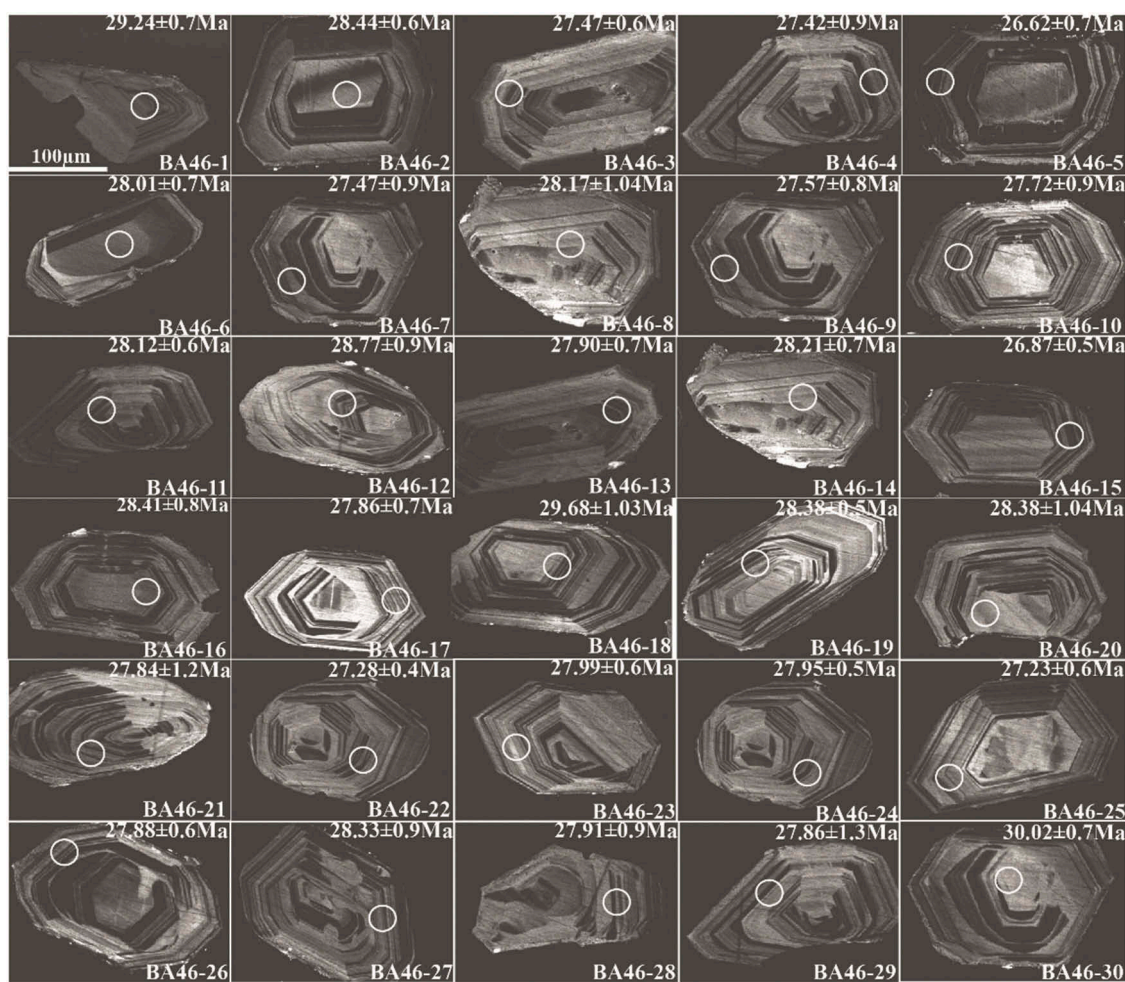


Figure 6. Cathodoluminescence (CL) images of zircon grains from granodiorite (sample BA46) in the Sarduiyeh granitoid rocks. The white circles show the sites of the SHRIMP spots, with age in Ma.

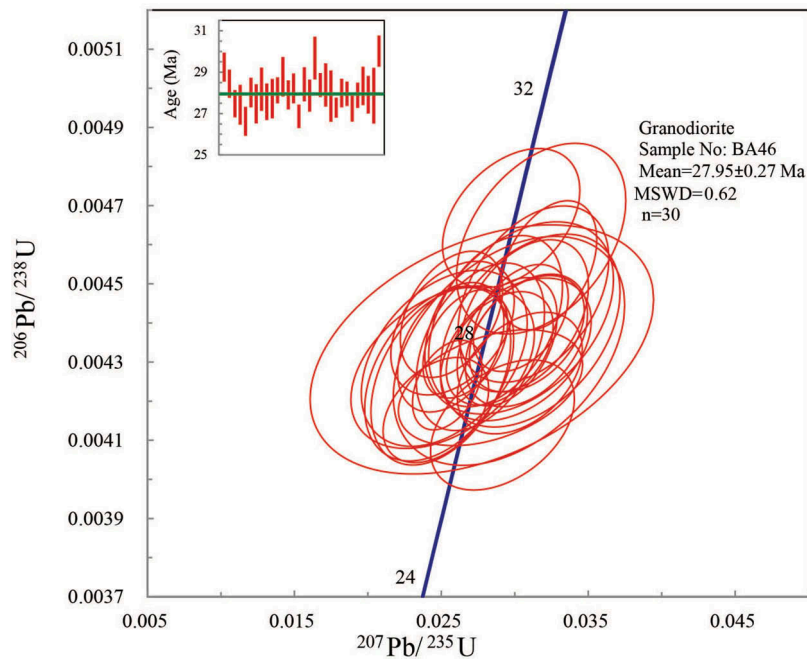


Figure 7. Concordia diagram of zircon U-Pb isotope data obtained by LA_ICPMS techniques for the granodiorite (sample BA46) in the Sarduiyeh granitoid rocks.

4.4. Whole-rock geochemistry

4.4.1. Major and trace element composition

Geochemical results show the LOI contents in the SG samples ranges between 0.39 to 2.62 wt. % which confirms the very low degree of alteration. The SiO_2 content varies between 55.14 and 73.87 wt.% (Supplementary Table 5). On the TAS diagram, the SG rocks plot in the diorite, granodiorite, granite fields that are in line with petrography studies (Figure 4) and show a subalkaline nature (Middlemost 1994; Figure 8(a)). The calc-alkaline nature of the SG is also clear on the AFM diagram (Figure 8(b)). In the A/CNK versus A/NK diagram (Figure 8(c)), all samples cluster in the metaluminous field.

On the Harker variation diagrams, the major and minor elements that are less affected by alteration are plotted against SiO_2 . The SG clearly exhibit a negative trends for MgO, FeO, Al_2O_3 , CaO, TiO_2 , P_2O_5 , Sr and Eu with increasing SiO_2 (Figure 9). In contrast, the K_2O and Y increase with SiO_2 variations (Figure 9(e–j)).

On N-MORB normalized spider diagrams, the SG form rather parallel patterns (Figure 10(a–d)). Diorite rocks are distinguished by the lowest trace element abundances. Tonalitic, granodioritic and monzogranitic samples show increasingly higher trace element abundances. So, trace element patterns of the SG rocks gradually increase from diorites to monzogranites. The SG show depletion in HFSE (such as Ti, Nb, Ta, Zr), and enrichment in large ion lithophile elements (LILE; K, Cs, Pb).

Chondrite normalized plot of REE for the SG shows light rare earth elements (LREE) enrichments (Figure 11(a–d)) with $(\text{La}/\text{Yb})_N = 2.44\text{--}8.68$ and flat heavy rare earth element (HREE) with $(\text{Gd}_N/\text{Yb}_N = 1.02\text{--}1.36$; Figure 11(a–d)). Most samples show strong to slight negative Eu anomalies $[(\text{Eu}/\text{Eu}^*)_N = 0.62\text{--}0.94]$ while few samples display slight positive Eu anomalies $[(\text{Eu}/\text{Eu}^*)_N = 1.004\text{--}1.24]$. In both spider and REE diagrams the various rock type in the SG follow the same general pattern of the Jebal Barez-type granitoids (Figure 10(a–d); Figure 11(a–d)).

4.4.2. Strontium and neodymium isotopic composition

Isotopic data from the SG are presented in supplementary Table 6. Their initial $^{87}\text{Sr}/^{86}\text{Sr}$ (I_{Sr}) and $^{143}\text{Nd}/^{144}\text{Nd}$ isotopic ratios were calculated using the zircon U-Pb ages of 27.95 Ma. The samples show uniform I_{Sr} from 0.7046 to 0.7049 and $(\epsilon_{\text{Nd}})_i$ values ranging from 3.4 to 4.03. The low variations in the I_{Sr} and positive ϵ_{Nd} between various SG rock types, points to their cogenetic relationships. Considering Nd model ages ($T_{\text{DM}i}$; De Paolo 1981), the results cluster around 425.29–738.56 Ma and $f\text{Sm}/\text{Nd}$ values limited to -0.16 to -0.45 (Supplementary Table 6).

5. Discussion

5.1. Petrogenesis

Field observations such as a close spatial association and gradual contacts between intermediate (diorite)

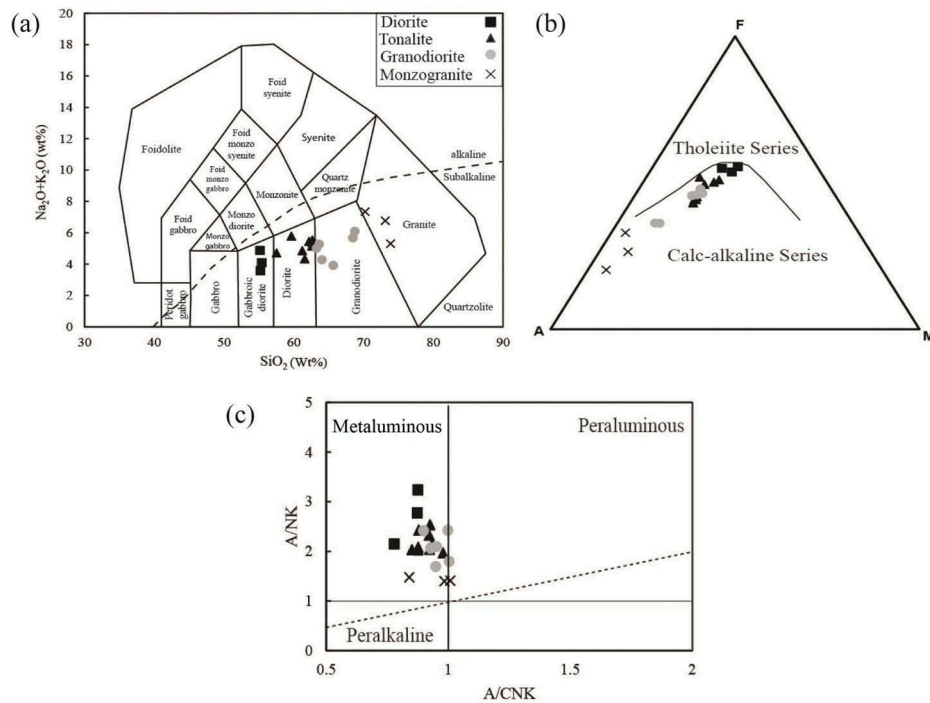


Figure 8. Classification of the Sarduiyeh granitoid rocks: (a) alkali versus silica diagram (Middlemost 1994), (b) ternary alkali-iron-magnesia (AFM) diagram (Irvin and Baragar 1971) and (c) plot of A/NK versus A/CNK [A/NK = molar Al₂O₃/(Na₂O + K₂O) and A/CNK = molar Al₂O₃/(CaO + Na₂O + K₂O)] diagram (Maniar and Piccoli 1989).

and felsic (tonalite, granodiorite and monzogranite) rocks reveal an intimate relationship between various rock types in the SG. Furthermore, some lines of geochemical evidences of SG rock types such as: rather similar REE patterns and Sr-Nd isotopic ratios accompanied by common calc-alkaline and metaluminous affinities of the rocks provide more confirmations that the intermediate and felsic rocks are co-magmatic.

The coherent trends on the Harker diagrams indicate that fractional crystallization has probably played a dominant role in the evolution of the SG (Figure 9). The sub parallel chondrite-normalized REE patterns and spider diagrams (Figures 10 and 11) for various SG rock types indicate their connections through fractional crystallization (Rapp and Watson 1995). On the REE diagrams the least fractionated samples (diorites) have the lowest REE pattern while the most evolved ones have higher REE contents. This is in agreement with a fractional crystallization link between the intermediate and felsic rocks. In addition to major and trace element geochemistry, the isotopic compositions of the SG are consistent with a fractional crystallization model. The plots of (⁸⁷Sr/⁸⁶Sr)_i and (¹⁴³Nd/¹⁴⁴Nd)_i versus SiO₂ clearly show that the fractional crystallization played a major role in the evolution of the SG magma (Figure 12(a,b)).

Most of the SG samples have negative Eu anomalies which can be explained by the role of plagioclase and/or K-feldspar during fractional crystallization

(Kebede and Koeberl 2003; Arslan and Aslan 2006; Zhong *et al.* 2009). However, few SG samples show a positive Eu anomaly (Figure 11(a-d)), which suggest feldspar accumulation. In the SG rocks Al₂O₃, Fe₂O₃, MgO, CaO, and TiO₂ decrease with increasing SiO₂ whereas the alkalis increase (Figure 9). These variations are consistent with petrographic observations, indicating that plagioclase, hornblende and magnetite have been the major differentiated phases (Kamgang *et al.* 2013).

In order to assess the types and quantities of fractionating mineral phases that were responsible for observed compositional variation in SG, the least-squares method was applied for the major elements (Cabero *et al.* 2012). In this model, the composition of least evolved diorite was considered to represent the parental magma (Supplementary Table 7, Figure 9, Cabero *et al.* 2012). Two stages of the crystal fractionation were calculated: (1) formation of granodiorite from diorite (2) formation of monzogranite from granodiorite. Fractional crystallization dominated by plagioclase (30%), amphibole (18%) and magnetite (4%) for the magmatic evolution from diorite to granodiorite. However fractional crystallization of a plagioclase (29%) dominated mineral assemblages that also include amphibole (8%), K-feldspar (7%), and magnetite (6%) controlled the evolutionary path from granodiorite to monzogranite.

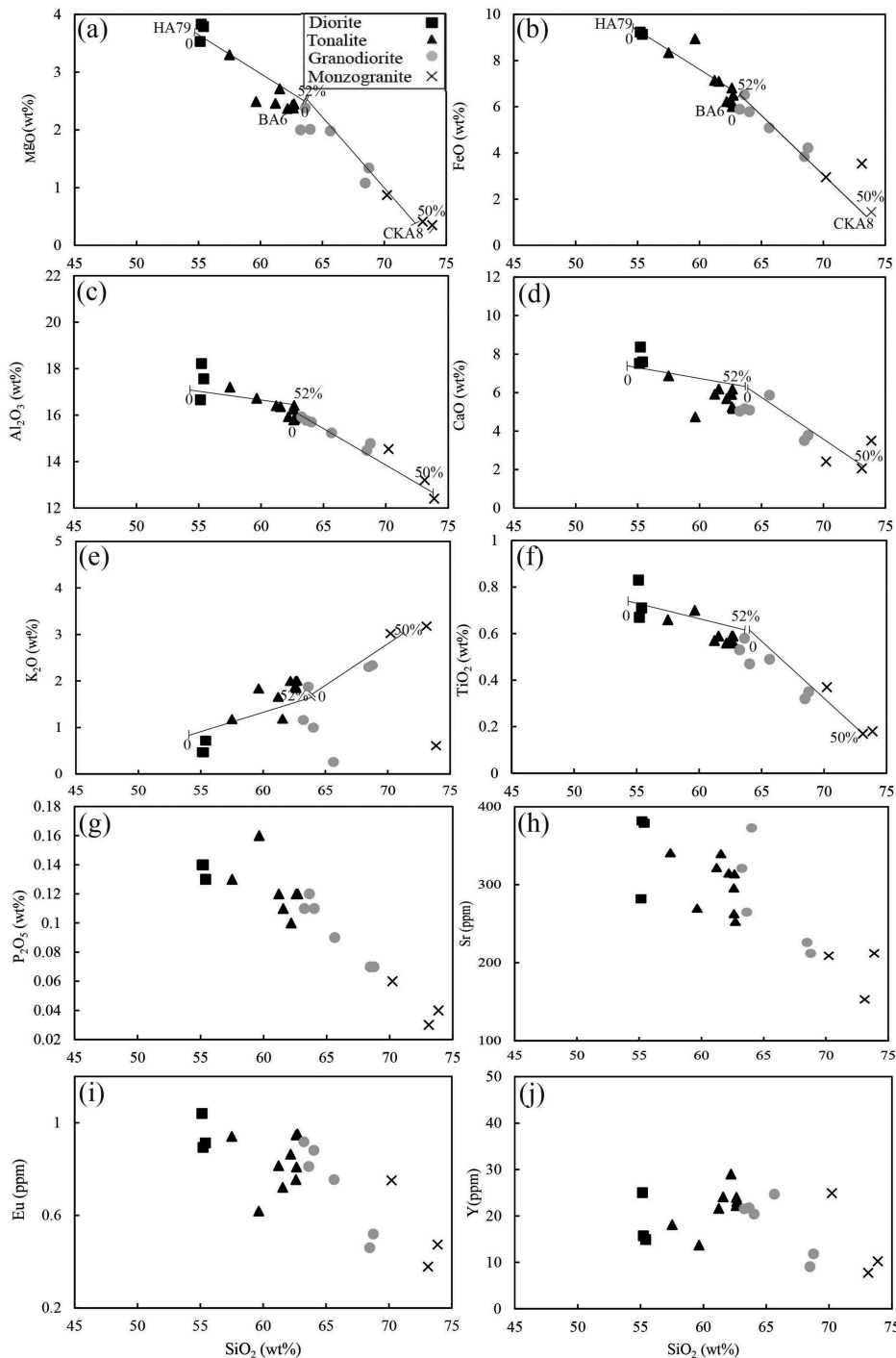


Figure 9. Binary plots of selected major element oxides and trace element versus SiO_2 content and least-squares fractional crystallization modelling trends (Supplementary Table 7) for the Sarduiyeh granitoid rocks. The trends show two stages of the crystal fractionation that led to the formation of granodiorite from diorite after 52% fractional crystallization dominated by: plagioclase (30%), amphibole (18%), magnetite (4%) and formation of monzogranite from granodiorite after 50% fractional crystallization dominated by: plagioclase (29%), amphibole (8%), K-feldspar (7%), magnetite (6%).

The zircon of the SG show positive Ce anomaly ($\text{Ce}/\text{Ce}^* = 2.85\text{--}41.63$) and negative Eu anomaly ($\text{Eu}/\text{Eu}^* = 0.007\text{--}0.364$) (Supplementary Figure 3) that may show a relatively oxidizing conditions for the SG parental magma (e.g. Guo *et al.* 1996; Hoskin and Schaltegger 2003).

Maas *et al.* (1992) suggested that oxygen fugacity is not the only factor controlling $\text{Eu}^{3+}/\text{Eu}^{2+}$ and $\text{Ce}^{4+}/\text{Ce}^{3+}$ ratios in magmas. The negative Eu anomalies may explain the important role of plagioclase fractionation in the magma, prior or during zircon crystallization (e.g. Hoskin *et al.* 2000).

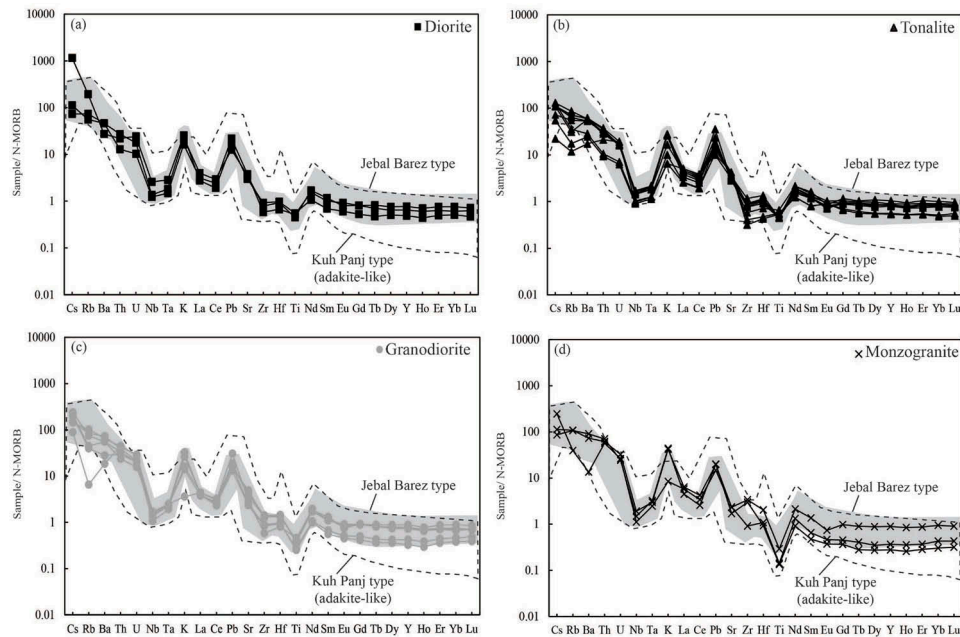


Figure 10. (a–d) N-MORB normalized plot of trace elements for the Sarduiyeh granitoid rocks. (N-MORB values from after Sun and McDonough 1989). The patterns for Jebal Barez and Kuh Panj granitoids from Asadi *et al.* (2014).

The $Sr/Y < 20$ (*av.* 16.35) and $La/Yb (N) < 20$ ratios, high Y (*av.* 19.35 ppm), low Sr content (*av.* 293.76 ppm) and low Cr and Ni contents (*av.* 20.1 and 4.69 ppm, respectively) of the SG demonstrate its normal calc-alkaline affinity (Defant and Drummond 1993). On the Sr/Y versus Y diagram, the SG samples plot on the normal calc-alkaline field (Defant and Drummond 1993; Figure 13). The non-adakitic geochemical characteristics of the SG resemble the Jebal Barez-type intrusions in the KCMA.

On the N-MORB normalized spider diagrams, the SG samples show depletion in HFSEs (such as Ti, Nb, Ta, Zr) and enrichment in LILEs (K, Cs, Pb). In destructive plate margin settings, the enrichments of magmatic rocks in LILEs, LREEs and depletion in Nb and Ta are typically attributed to the metasomatism of their mantle wedges by fluids derived from the down going slabs (e.g. Zhou *et al.* 2006). However, some geochemical characteristics of the SG such as: low Mg# (10.4–29.33), very low Cr (10.9–42.5 ppm) and Ni contents (1.8–10.7 ppm) (Supplementary Table 5) (which are much lower than those which is expected for mantle derived primary melts (Mg# 73–81, Ni >400 ppm and Cr >1000 ppm) (Wilson 1989) plus high SiO_2 content (55.14–73.87 wt%) contradict generation SG parental magma from a metasomatized mantle wedge. Alternatively, the lower crust might be a plausible source for the SG parental magma, as negative anomalies for Nb, Ta, and Ti has been reported for the crustal melt (Rudnick and Fountain 1995).

Some trace element ratios, such as Y/Nb and Nb/La remain unaffected during fractional crystallization and

thus are useful for identifying magma sources (Eby 1992; Morata *et al.* 2005). Eby (1992) noted that granitoids that evolved from mantle derived melt have $Y/Nb < 1.2$, in contrast to those crustal derived melt which have $Y/Nb > 1.2$. The SG samples have $Y/Nb = 2.24–11.01$ which suggest a crustal origin for the SG. Moreover, the average Nb/La ratio of primitive mantle and continental rock is 1.01 and 0.46, respectively (McDonough *et al.* 1992; Morata *et al.* 2005). The Nb/La ratio for SG ranges from 0.1 to 0.4 (*av.* 0.34) which is close to the value reported for lower crustal derived magmas. So, these incompatible trace element ratios show a crustal origin for the SG.

On the $\epsilon Nd (i)$ versus ISr diagram (Figure 14), the SG rocks plot close to the mantle array (with Jebal Barez-type overlapping). In addition, the SG samples fall near the line of average crust ($K/Rb = 250$) in Taylor and McLennan (1985) diagram which suggest a crustal origin for the SG magma (Figure 15(a)). Patino Douce (1999) presented a discrimination diagram based on major element combinations to identify the relative contributions of metasedimentary and mafic sources to granitic melts (Figure 15(b)). On the $Al_2O_3 / (FeO_t + MgO + TiO_2)$ versus $Al_2O_3 + FeO_t + MgO + TiO_2$ diagram, the SG samples plot in the amphibolite-derived melt field.

As mentioned above, the geochemical characteristics clearly propose a crustal origin for the SG. The $Na_2O > K_2O$, molecular $A/CNK < 1$ ratio, an increasing trend of Y versus SiO_2 and presence of key minerals such as hornblende and biotite all are supporting the I-type characteristic of SG (White and Chappell 1983; Harris *et al.* 1986). I-type

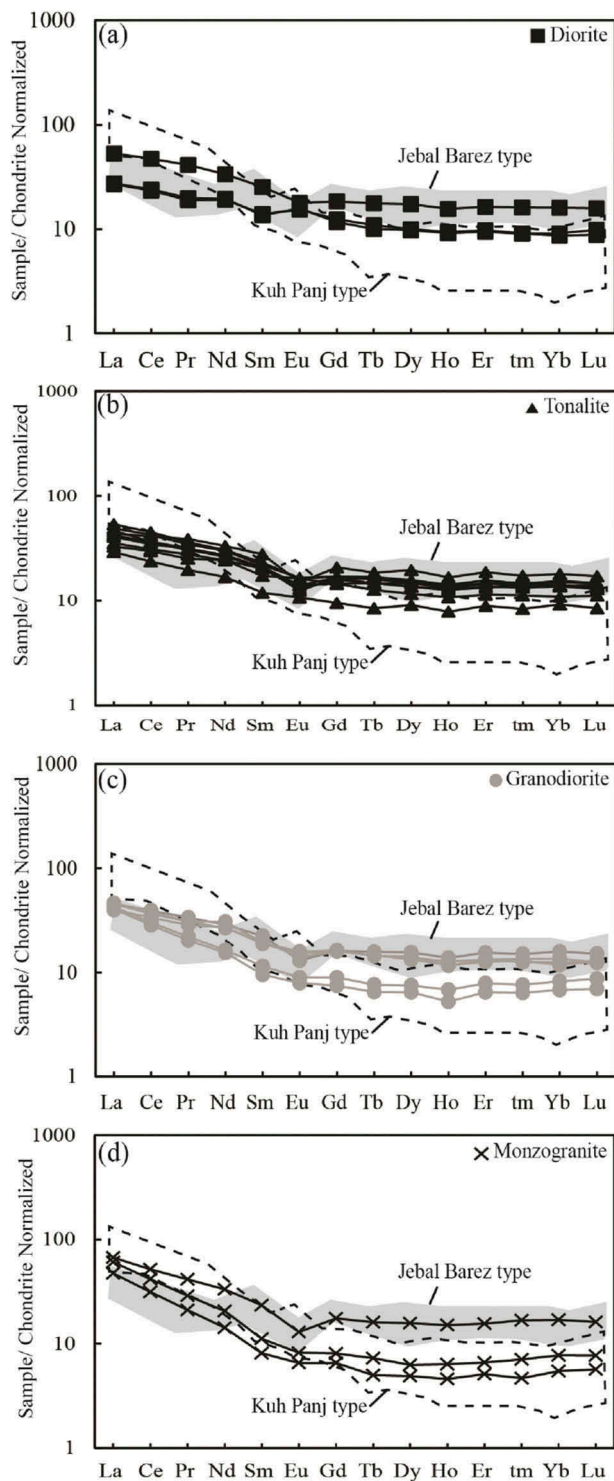


Figure 11. (a–d) Chondrite-normalized rare earth element patterns for the Sarduiyeh granitoid rocks. Normalization factors from after Sun and McDonough (1989). The patterns for Jebal Barez and Kuh Panj granitoids from Asadi *et al.* (2014).

plutonic rocks are inferred to have formed from a metabasic rocks of lower crust. The flat HREE patterns indicate that garnet was not a residual mineral during partial melting of the crust (Rapp and Watson 1995).

6. Thermobarometry

Geothermobarometry can be helpful in monitoring temperature and pressure under which magma has been evolved. Thermometry based on chemical composition of amphibole and plagioclase is a very important tool for estimation of crystallization temperatures of igneous rocks. Using amphibole-plagioclase thermometry of Holland and Blundy (1994) the SG yielded temperature of 730–850°C.

The barometry based on the Al content in hornblende has been widely used to infer magmatic crystallization pressure (Anderson and Smith 1995). Al-hornblende barometry must be used only in the presence of suitable mineral assemblages in granitoid rocks (quartz + plagioclase + alkali feldspar + biotite + hornblende + titanite + magnetite or ilmenite) which clearly limits compositional influences (Helmy *et al.* 2004). Al-in-hornblende barometry demonstrates a pressure estimation of 1–3 kbar for the SG.

The zircon saturation thermometry that was introduced by Watson and Harrison (1983) has been widely used as a tool to estimate the crystallization temperature of zircon in Zr-saturated granite melts. Watson and Harrison (1983) stated that the saturation of zircon, as a function of melt composition and temperature, can be yielded using the $\ln D_{Zr}^{(zircon/melt)} = (-3.80 - [0.85(M-1)]) + 12,900/T$ equation. In this equation M stands for $(K + Na + 2Ca)/(Si.Al)_{cat}$ and temperature is in Kelvin. The proposed equation is only applicable for whole rocks with M value of 0.9–1.7. In this context, only monzogranites of SG are suitable that yield a restricted temperature range ($T_{Zr} = 801\text{--}803^\circ\text{C}$). Miller *et al.* (2003) distinguished inheritance-rich and inheritance-poor granitoid that their zircon saturation temperatures are 766°C and 837°C, respectively. Referring to the obtained T_{Zr} for SG, it is clear that they belong to inheritance-poor granitoids.

7. Tectonic setting

The granitoid tectonic discrimination diagrams display a continental arc setting for the SG rock types. They plot on the Nb versus Y and Ta versus Yb discrimination diagrams (Pearce *et al.* 1984), clearly show the volcanic arc affinity, as is expected for UDMA continental arc magmatism (Figure 16(a,b)). This is in line with arc like geochemical features of SG (Figures 10 and 11) such as fractionated REE patterns, enriched LILEs and depleted HFSEs (Figures 10 and 11). The arc signature of SG is also clear in Y versus Zr (Muller 1995) and in Rb/Zr versus Nb

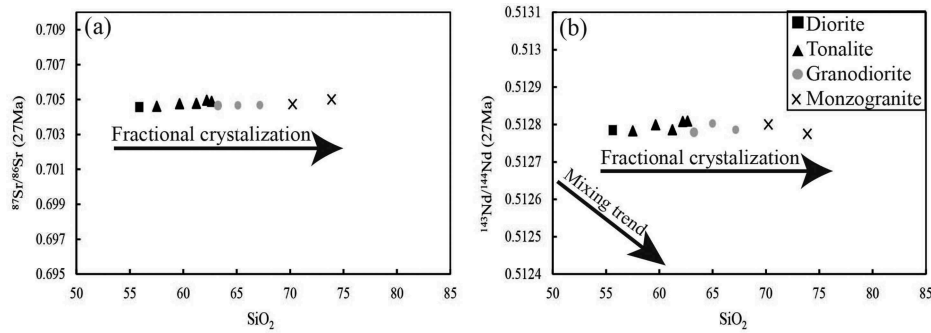


Figure 12. SiO_2 versus (a) $(^{87}\text{Sr}/^{86}\text{Sr})_i$ and (b) $(^{143}\text{Nd}/^{144}\text{Nd})_i$ diagrams (after Wang *et al.* 2006) for Sarduiyeh granitoid rocks, showing the possible magmatic processes that are predominant during the magma evolution.

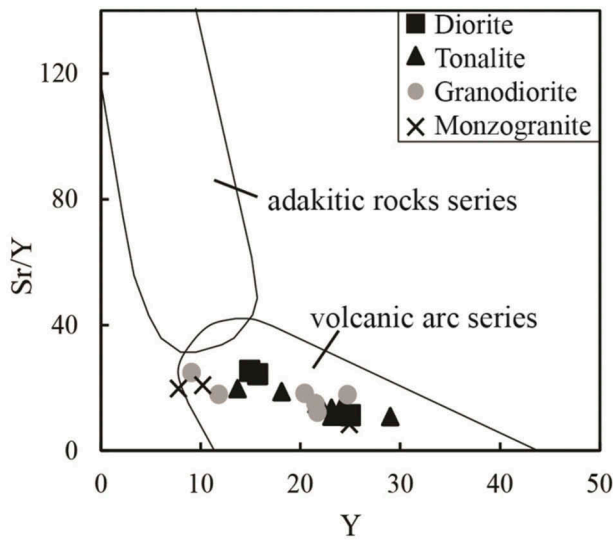


Figure 13. Sr/Y versus Y diagram showing volcanic arc affinity of Sarduiyeh granitoid rocks (after Defant and Drummond 1993).

(Brown *et al.* 1984) diagrams where the samples plot in the arc-related magmatic field and the primitive continental arc field, respectively (Figure 16 (c,d)).

It is commonly accepted that the subduction of the Neo-Tethys oceanic lithosphere underneath the Central Iranian microcontinent continued from Mid-Late Mesozoic to Late Oligocene-Early Miocene. This led to partial melting of mantle wedge (metasomatized by aqueous fluids derived from the down going oceanic slab) and as a consequence the Mesozoic and Early Cenozoic Andean-type arc magmatism in the SSZ and UDMA (Berberian *et al.* 1982; Mohajjel *et al.* 2003; Alavi 2007; Agard *et al.* 2011; Chiu *et al.* 2013; Shafaii Moghadam *et al.* 2015). In the KCMA, the non-adakitic Jebal Barez type is considered as the pre-collision evolved product of mantle derived melts via extensive subsequent fractionation, whereas the adakitic Kuh Panj type is explained by melting of a thickened garnet bearing crustal source in a post-collision tectonic setting (Asadi *et al.* 2014;

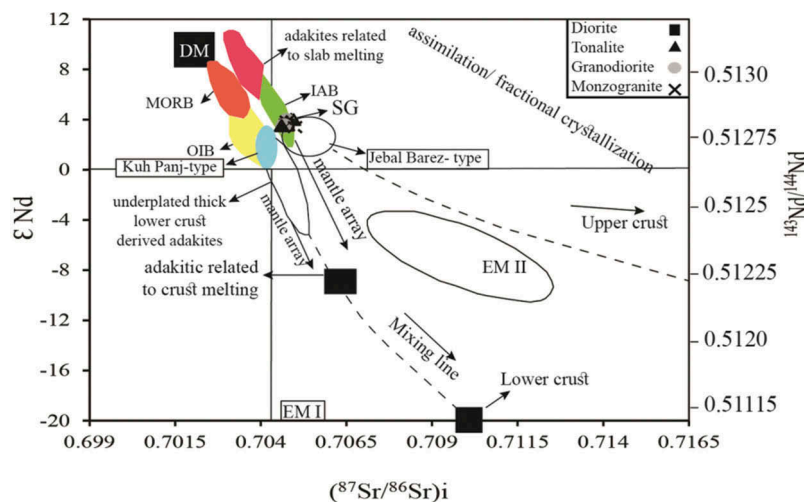


Figure 14. ϵNd (i) versus initial $^{87}\text{Sr}/^{86}\text{Sr}$ diagram for the Sarduiyeh granitoid rocks. The field of adakites related to slab melting is defined after Defant *et al.* (1992); Kay *et al.* (1993); Sajona *et al.* (2000). The data for underplated thick lower crust adakites are after Atherton and Petford (1993); Muir *et al.* (1995) and Petford and Atherton (1996). The data for adakites related to crust melting are after Hou *et al.* (2011). Abbreviations: MORB: Mid-ocean ridge basalts; OIB: ocean-island basalts; DM: depleted mantle; IAB: island-arc basalts after Zindler and Hart (1986); EM I and EM II two types of enriched mantle end-members, (Hou *et al.* 2011). The fields for Jebal Barez and Kuh-Panj granitoids from Asadi *et al.* (2014).

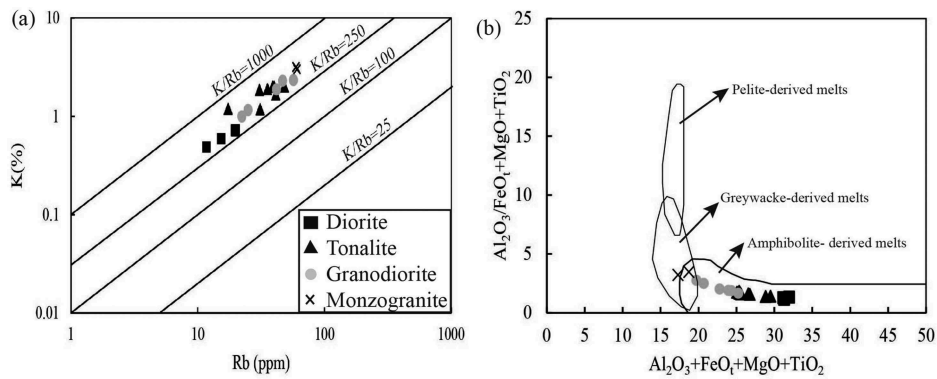


Figure 15. (a) K versus Rb variation diagram for the SG. The samples plot near the line of average continental crust ($K/Rb = 250$) of after Taylor and McLennan (1985). (b) Compositional comparison between SG samples and partial melts obtained in experimental studies by dehydration melting of various bulk compositions including felsic pelites, metagreywackes and amphibolites (after Patino Douce 1999; modified by Chen *et al.* 2016).

Chekani Moghadam *et al.* 2017). The geochemical and zircon U-Pb age data presented in this study clearly show that the SG belongs to the Jebal Barez-type intrusions. However, geochemical characteristics of the SG rule out partial melting of a metasomatized mantle wedge as a plausible source for its magma and rather than support a partial melting from metabasic rocks of lower crust. The most anticipated heat source for partial melting has been provided by hot basaltic melt from the partial melting of metasomatized mantle wedge that in its route to the surface may pond at the base of the overlying lower crust due to gravity constraints, causing partial melting lower crust metabasic rocks. These processes together with fractional

crystallization formed the Jebal Barez-type SG with typical calc-alkaline affinity. This geodynamic setting is schematically illustrated in Figure 17.

8. Conclusions

The medium-to-coarse-grained Sarduiyeh granitoid is located in the southeastern part of the UDMA. The granular texture granitoid consists mainly of diorite, tonalite, granodiorite and monzogranitic rocks. The geochemical studies indicate that the SG is calc-alkaline, I-type, metaluminous, enriched in LILE (such as K, Cs, Pb) and depleted in HFSE (such as Ti, Nb, Ta, Zr).

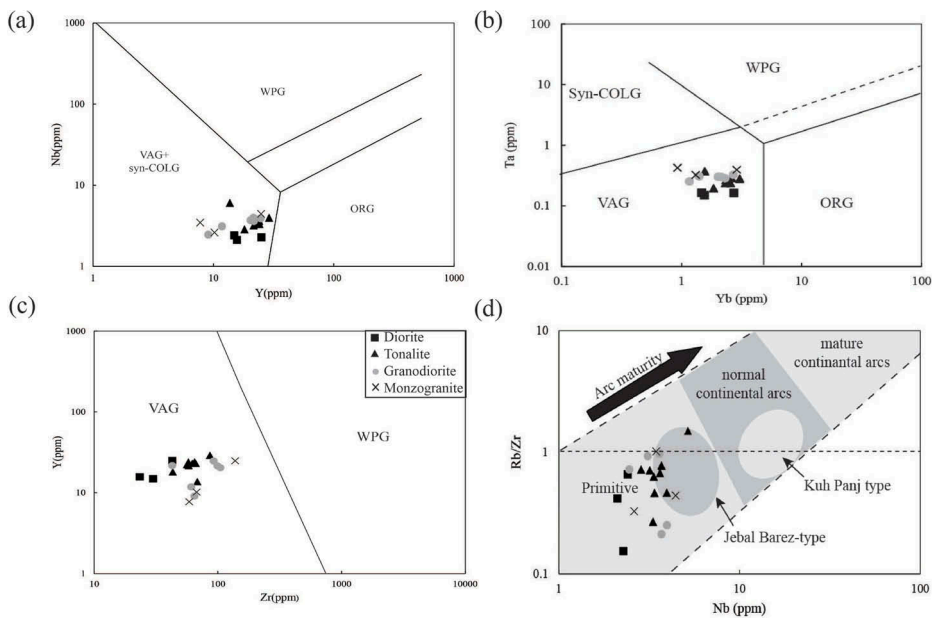


Figure 16. The plots of the Sarduiyeh granitoid rocks: on (a, b) tectonic discrimination diagrams of after Pearce *et al.* (1984) Syn-COLG (Syncollisional), VAG (Volcanic arc), WPG (Within-plate) and ORG (Ocean-ridge). (c) Zr versus Y diagram of after Muller (1995) (d) Rb/Zr versus Nb diagram of after Brown *et al.* (1984). The fields for Jebal Barez and Kuh-Panj granitoids from Asadi *et al.* (2014).

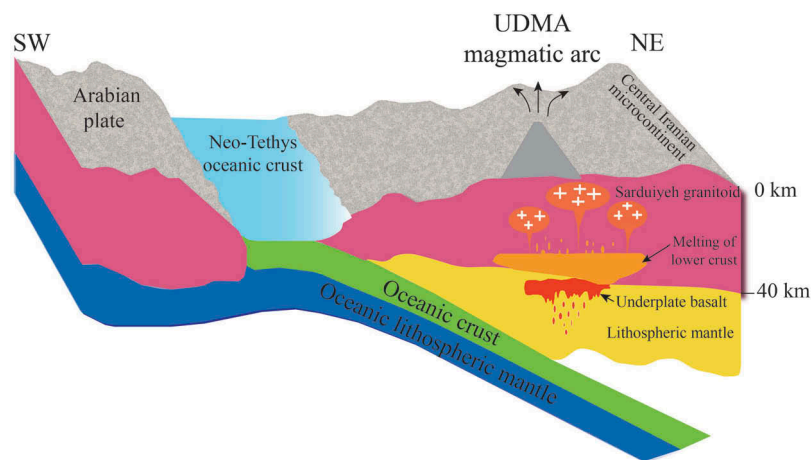


Figure 17. Tectonic model for the generation of the Jebal-Barez type calc-alkaline granitoids in late Oligocene time. The most anticipated heat source for partial melting has been provided by hot basaltic melt from the partial melting of metasomatized mantle wedge that in its route to the surface may pond at the base of the overlying lower crust due to gravity constraints, causing partial melting lower crust metabasic rocks. Consequently, these processes together with fractional crystallization may have formed the Jebal Barez-type Sarduiyeh granitoid (see text for the details).

Chondrite normalized plot of SG rare earth elements show LREE enrichments with ($La_N/Yb_N = 2.44\text{--}8.68$) and flat heavy rare earth element patterns with ($Gd_N/Yb_N = 1.02\text{--}1.36$). This interpretation is further supported by the ASI frequency distribution of less than 1 and presence of key minerals such as hornblende and biotite. The rather high Y (av. 19.35 ppm), low Sr content (av. 293.76 ppm) and low Cr and Ni contents (av. 20.1 and 4.69 ppm, respectively) of the SG demonstrate its normal calc-alkaline and non-adakitic affinity, the features of Jebal Barez-type granitoids. The use of tectonic discrimination diagrams of granitoids reveals that the SG was emplaced in a continental arc regime during subduction of the Neo-Tethys oceanic lithosphere underneath the Central Iranian microcontinent. The very low Cr and Ni contents, low Mg# (av. 25.24 ppm) and isotopic data ($(\epsilon_{Nd})_i = +3.4$ to $+4.03$, and $I_{Sr} 0.7046$ to 0.7049) show that the SG was generated by partial melting of meta-basic (amphibolite) rocks at lower crust. P-T calculations based on hornblende barometry and amphibole-plagioclase thermometry suggested an approximate pressure of 1–3 Kbar and crystallization temperature of about 730–850°C for the SG. The sub parallel chondrite-normalized REE patterns and spider diagrams for various rock types indicate their connections through fractional crystallization. The zircon U-Pb age of 27.95 ± 0.27 Ma suggest a per-plate collision for the formation of the SG. It also shows that the final collision between the Arabian plate and Central Iranian microcontinent may have happened in the Late Oligocene.

Acknowledgements

The present study is a part of the first author's PhD thesis at Hormozgan University, Iran. We wish to thank the National Iranian Copper Industries Company (NICICO) for their financial supports. We also thank Dr. Zhouting and the Institute of Geochemistry Chinese Academy of Sciences in Guiyang for analytical assistance and isotope analysis. The authors gratefully acknowledge Dr Hossein Azizi, Dr Hadi Shafaii Moghadam and two anonymous reviewers for their constructive comments on the manuscript. We also appreciate the very helpful suggestions and comments by the Editor-in-Chief Professor Stern.

Disclosure statement

No potential conflict of interest was reported by the authors.

References

- Agard, P., Omrani, J., Jolivet, L., and Mouthereau, F., 2005, Convergence history across Zagros (Iran): constraints from collisional and earlier deformation: *International Journal of Earth Sciences*, 94, 401–419. Doi: [10.1007/s00531-005-0481-4](https://doi.org/10.1007/s00531-005-0481-4)
- Agard, P., Omrani, J., Whitechurch, H., Vrielynck, B., Spakman, W., Monie, P., Meyer, B., and Wortel, R., 2011, Zagros orogeny: a subduction-dominated process: *Geological Magazine*, 148, 692–725. Doi: [10.1017/S001675681100046X](https://doi.org/10.1017/S001675681100046X)
- Aghazadeh, M., Hou, Z., Badrzadeh, Z., and Zhou, L., 2015, Temporal-spatial distribution and tectonic setting of porphyry copper deposits in Iran: constraints from zircon U-Pb and molybdenite Re-Os geochronology: *Ore Geology Reviews*, 70, 385–406. Doi: [10.1016/j.oregeorev.2015.03.003](https://doi.org/10.1016/j.oregeorev.2015.03.003)
- Ahmad, T., and Posht Kuhi, M., 1993, Geochemistry and petrogenesis of Urumieh-Dokhtar volcanic belt around Nain

- and Rafsanjan area; a preliminary study: treatise on the geology of Iran: Iranian Ministry of Mines and Metals, 4, 90
- Alavi, M., 1994, Tectonics of the Zagros orogenic belt of Iran: new data and interpretations: *Tectonophysics*, 229, 211–238. Doi: [10.1016/0040-1951\(94\)90030-2](https://doi.org/10.1016/0040-1951(94)90030-2)
- Alavi, M., 1996, Tectonostratigraphic synthesis and structural style of the Alborz mountain system in Iran: *Journal of Geodynamics*, 21, 1–33
- Alavi, M., 2004, Regional stratigraphy of the Zagros folded-thrust belt of Iran and its proforeland evolution: *American Journal of Science*, 304, 1–20. Doi: [10.2475/ajs.304.1.1](https://doi.org/10.2475/ajs.304.1.1)
- Alavi, M., 2007, Structure of the Zagros fold-thrust belt in Iran: *American Journal of Science*, 307, 1064–1095. Doi: [10.2475/09.2007.02](https://doi.org/10.2475/09.2007.02)
- Anderson, J.L., and Smith, D.R., 1995, The effects of temperature and FO_2 on the Al-in Hornblende barometer: *American Mineralogist*, 80, 549–559. Doi: [10.2138/am-1995-5-614](https://doi.org/10.2138/am-1995-5-614)
- Arslan, M., and Aslan, Z., 2006, Mineralogy, petrography and whole-rock geochemistry of the tertiary granitic intrusions in the Eastern Pontides, Turkey: *Journal of Asian Earth Sciences*, 27, 177–193. Doi: [10.1016/j.jseaes.2005.03.002](https://doi.org/10.1016/j.jseaes.2005.03.002)
- Arvin, M., Pan, Y., Dargahi, S., Malekizadeh, A., and Babaei, A., 2007, Petrochemistry of the Siah-Kuh granitoid stock southwest of Kerman, Iran: implications for initiation of Neotethys subduction: *Journal of Asian Earth Sciences*, 30, 474–489. Doi: [10.1016/j.jseaes.2007.01.001](https://doi.org/10.1016/j.jseaes.2007.01.001)
- Asadi, A., Moore, F., and Zarasvandi, A., 2014, Discriminating productive and barren porphyry copper deposits in the southeastern part of the central Iranian volcano – Plutonic belt, Kerman region, Iran: a review: *Earth Science Reviews*, 138, 25–46. Doi: [10.1016/j.earscirev.2014.08.001](https://doi.org/10.1016/j.earscirev.2014.08.001)
- Atherton, M.P., and Petford, N., 1993, Generation of sodium-rich magmas from newly underplated basaltic crust: *Nature*, 362, 144–146. Doi: [10.1038/362144a0](https://doi.org/10.1038/362144a0)
- Azizi, H., Asahara, Y., Mehrabi, B., and Chung, S.L., 2011, Geochronological and geochemical constraints on the petrogenesis of high-K granite from the Suffiabad area, Sanandaj-Sirjan Zone, NW Iran: *Chemie der Erde*, 71, 363–376. Doi: [10.1016/j.chemer.2011.06.005](https://doi.org/10.1016/j.chemer.2011.06.005)
- Bahroudi, A., and Talbot, C.J., 2003, The configuration of the basement beneath the Zagros basin: *Journal of Petroleum Geology*, 26, 257–282. Doi: [10.1111/jpg.2003.26.issue-3](https://doi.org/10.1111/jpg.2003.26.issue-3)
- Belousova, E.A., Griffin, W.L., Suzanne, Y.O.R., and Fisher, N.I., 2002, Igneous zircon: trace element composition as an indicator of source rock type: *Contributions to Mineralogy and Petrology*, 143, 602–622. Doi: [10.1007/s00410-002-0364-7](https://doi.org/10.1007/s00410-002-0364-7)
- Berberian, F., and Berberian, M., 1981, Tectono-plutonic episodes in Iran, in Gupta, H.K., and Delany, F.M. eds., *Zagros, Hindukosh, Himalaya geodynamic evolution*: Washington, DC, American Geophysical Union, 5–32
- Berberian, F., Muir, I.D., Pankhurst, R.J., and Berberian, M., 1982, Late Cretaceous and early Miocene Andean-type plutonic activity in northern Makran and Central Iran: *Journal of the Geological Society of London*, 139, 605–614. Doi: [10.1144/gsjgs.139.5.0605](https://doi.org/10.1144/gsjgs.139.5.0605)
- Berberian, M., and King, G.C.P., 1981, Towards a paleogeography and tectonic evolution of Iran: *Canadian Journal of Earth Sciences*, 18, 210–265. Doi: [10.1139/e81-019](https://doi.org/10.1139/e81-019)
- Brown, G.C., Thorpe, R., and Webb, P.C., 1984, The geochemical characteristics of granitoids in contrasting arc and comments on magma source: *Journal of the Geological Society of London*, 141, 413–426. Doi: [10.1144/gsjgs.141.3.0413](https://doi.org/10.1144/gsjgs.141.3.0413)
- Bushara, M.N., 1995, Subsurface structure of the eastern edge of the Zagros basin as inferred from gravity and satellite data: *American Association of Petroleum Geologist Bulletin*, 79, 1259–1273
- Cabero, M.T., Mecoleta, S., and Lopez-Moro, F.J., 2012, OPTIMASBA: a Microsoft Excel workbook to optimise the mass-balance modelling applied to magmatic differentiation processes and subsolidus overprints: *Computers and Geoscience*, 42, 206–211. Doi: [10.1016/j.cageo.2011.10.013](https://doi.org/10.1016/j.cageo.2011.10.013)
- Chekani Moghadam, M., Tahmasbi, Z., Ahmadi Khalaji, A., and Santos, J.F., 2017, Petrogenesis of Rabor-Lalehzar magmatic rocks (SE Iran): constraints from whole rock chemistry and Sr-Nd isotopes: *Chemie der Erde*, 78, 58–77. Doi: [10.1016/j.chemer.2017.11.004](https://doi.org/10.1016/j.chemer.2017.11.004)
- Chen, M., Sun, M., Buslov, M.M., Cai, K., Zhao, G., Kulikova, A. V., and Rubanova, E.S., 2016, Crustal melting and magma mixing in a continental arc setting: evidence from the Yaloman intrusive complex in the Gorny Altai terrane, Central Asian Orogenic Belt: *Lithos*, 252, 76–91. Doi: [10.1016/j.lithos.2016.02.016](https://doi.org/10.1016/j.lithos.2016.02.016)
- Chiu, H.Y., Chung, S.L., Zarrinkoub, M.H., Mohammadi, S.S., Khatib, M.M., and Lizuka, Y., 2013, Zircon U-Pb age constraints from Iran on the magmatic evolution related to Neotethyan subduction and Zagros orogeny: *Lithos*, 162–163, 70–87. Doi: [10.1016/j.lithos.2013.01.006](https://doi.org/10.1016/j.lithos.2013.01.006)
- Clarke, B.D., 1992, *Granitoid rocks*: Chapman and Hall Publisher, London, 283
- Cobbing, J., 1996, *Granites: an overview*: Episodes-News magazine of the International Union Geological Sciences, 19, 103–106
- Colman Sadd, S., 1978, Fold development in Zagros simply folded belt southwest Iran: *American Association of Petroleum Geologist Bulletin*, 62, 984–1003
- Conrad, G., Conrad, J., and Girod, M., 1977, Les formations continentales tertiaires et quaternaires du bloc du lout (Iran): importances du plutonisme et du volcanisme: *Mémoires de la Société géologique de France*, 8, 53–75
- Corfu, F., Hanchar, J.M., Hoskin, P.W., and Kinny, P., 2003, Atlas of zircon textures: *Reviews in Mineralogy and Geochemistry*, 53, 469–500. Doi: [10.2113/0530469](https://doi.org/10.2113/0530469)
- Dargahi, S., 2007, Miocene post-collision magmatism in region between Sar Cheshmeh and Shahr Babak, southwestern Kerman: investigation of isotopic data, petrogenetic analysis, geodynamic model for granitoid bodies, and role of adakitic magmatism in development of copper mineralization [Unpublished PhD thesis], Shahid Bahonar University of Kerman, 306p.
- Dargahi, S., Arvin, M., Pan, Y., and Babaei, A., 2010, Petrogenesis of post-collisional A-type granitoids from the Urumieh-Dokhtar magmatic assemblage, southwestern Kerman, Iran: constraints on the Arabian-Eurasian continental collision: *Lithos*, 115, 190–204. Doi: [10.1016/j.lithos.2009.12.002](https://doi.org/10.1016/j.lithos.2009.12.002)
- De Paolo, D.J., 1981, Trace-element and isotopic effects of combined wall rock assimilation and fractional crystallization: *Earth and Planetary Science Letters*, 53, 189–202. Doi: [10.1016/0012-821X\(81\)90153-9](https://doi.org/10.1016/0012-821X(81)90153-9)
- Deer, W.A., Howie, R.A., and Zussman, J., 1992, *An introduction to the Rock-Forming Minerals*: Longman, London, 696

- Defant, M.J., and Drummond, M.S., 1993, Mount St. Helens: potential example of the partial melting of the subducted lithosphere in a volcanic arc: *Geology*, 21, 547–550. Doi: [10.1130/0091-7613\(1993\)021<0547:MSHPEO>2.3.CO;2](https://doi.org/10.1130/0091-7613(1993)021<0547:MSHPEO>2.3.CO;2)
- Defant, M.J., Jackson, T.E., Drummond, M.S., De Boer, J.Z., Bellon, H., Feigenson, M.D., Maury, R.C., and Stewart, R.H., 1992, The geochemistry of young volcanism throughout western Panama and southeastern Costa Rica, an overview: *Journal of the Geological Society of London*, 149, 569–579. Doi: [10.1144/gsjgs.149.4.0569](https://doi.org/10.1144/gsjgs.149.4.0569)
- Dercourt, J., Zonenshain, L., Ricou, L.E., Kazmin, G., Lepichon, X., Knipper, A.L., Granjacquet, C., Sbotshikov, I.M., Geyssant, J., Lepvrier, C., Pechersky, D.H., Boulin, J., Sibuet, J.C., Savostin, L. A., Sorokhtin, O., Westphal, M., Bazhenov, M.L., Lauer, J.P., and Biju-Duval, B., 1986, Geological evolution of the Tethys belt from the Atlantic to Pamir's since the Lias: *Tectonophysics*, 123, 241–315. Doi: [10.1016/0040-1951\(86\)90199-X](https://doi.org/10.1016/0040-1951(86)90199-X)
- Dimitrijevic, M.D., 1973, Sarduiyeh geological map: Iran Geological Survey, scale 1:100 000, 1 sheet, sheet 7448
- Eby, G.N., 1992, Chemical subdivision of the A-type granitoids: petrogenetic and tectonic implications: *Geology*, 20, 641–644. Doi: [10.1130/0091-7613\(1992\)020<0641:CSOTAT>2.3.CO;2](https://doi.org/10.1130/0091-7613(1992)020<0641:CSOTAT>2.3.CO;2)
- Emami, M.H., Sadeghi, M., and Omrani, J., 1993, Iran Magmatic map: Iran Geological Survey, scale 1:2 500 000, 1 sheet
- Ghorashi Zadeh, M., 1978, Development of hypogene and supergene alteration and copper mineralization patterns, Sar Cheshmeh porphyry copper deposit, Iran [Unpublished M.Sc thesis], Brock University of Canada, 223p.
- Glennie, K.W., 2000, Cretaceous tectonic evolution of Arabia's eastern plate margin: a tale of two oceans, in *Middle East models of Jurassic/Cretaceous carbonate systems: Middle East Models of Jurassic/ Cretaceous Carbonate System*, Society of Economic Paleontologists and Mineralogists, Special Publication, 69, 9–20 Doi: [10.2110/pec.00.69.0009](https://doi.org/10.2110/pec.00.69.0009)
- Golonka, J., 2004, Plate tectonic evolution of the Southern margin of Eurasia in the Mesozoic and Cenozoic: *Tectonophysics*, 381, 235–273. Doi: [10.1016/j.tecto.2002.06.004](https://doi.org/10.1016/j.tecto.2002.06.004)
- Guo, J., O'Reilly, S.Y., and Griffin, W.L., 1996, Zircon inclusions in corundum megacrysts: I. Trace element geochemistry and clues to the origin of corundum megacrysts in alkali basalts: *Geochimica et Cosmochimica Acta*, 60, 2347–2363. Doi: [10.1016/0016-7037\(96\)00084-1](https://doi.org/10.1016/0016-7037(96)00084-1)
- Harris, N.B.W., Pearce, J.A., and Tindle, A.G., 1986, Geochemical characteristics of collision-zone magmatism, in Coward, M. P., and Ries, A.C., eds., *Collision Tectonics: Geological Society of London, Special Publication*, Vol. 19, 67–81. Doi: [10.1144/gsl.sp.1986.019.01.04](https://doi.org/10.1144/gsl.sp.1986.019.01.04)
- Hassanzadeh, J., 1993, Metallogenic and tectono-magmatic events in the SE sector of the Cenozoic active continental margin of Iran (Shahre Babak area, Kerman province) [Unpublished PhD thesis], University of California, 204p.
- Helmy, H.M., Ahmed, A.F., ElMahallawi, M.M., and Ali, S.M., 2004, Pressure, temperature and oxygen fugacity conditions of calc-alkaline granitoids, Eastern Desert of Egypt, and tectonic implication: *Journal of African Earth Sciences*, 38, 255–268. Doi: [10.1016/j.jafrearsci.2004.01.002](https://doi.org/10.1016/j.jafrearsci.2004.01.002)
- Holland, T., and Blundy, J., 1994, Non-ideal interactions in calcic amphiboles and their bearing on amphibole-plagioclase thermometry: *Contribution to Mineralogy and Petrology*, 116, 433–447. Doi: [10.1007/BF00310910](https://doi.org/10.1007/BF00310910)
- Hoskin, P.W.O., and Schaltegger, U., 2003, The composition of zircon and igneous and metamorphic petrogenesis, in Hanchar, J., and Hoskin, P.W.O., eds., *Zircon: mineralogical Society of America and Geochemical Society: Reviews in Mineralogy and Geochemistry*, Vol. 53, 27–62. Doi: [10.2113/0530027](https://doi.org/10.2113/0530027)
- Hoskin, P.W.O., Kinny, P.D., Wyborn, D., and Chappell, B.W., 2000, Identifying accessory mineral saturation during differentiation in granitoid magmas: an integrated approach: *Journal of Petrology*, 41, 1365–1369. Doi: [10.1093/petrology/41.9.1365](https://doi.org/10.1093/petrology/41.9.1365)
- Hou, Z.Q., Zhang, H., Pan, X., and Yang, Z., 2011, Porphyry Cu (Mo-Au) deposits related to melting of thickened mafic lower crust: examples from the eastern Tethyan metallogenic domain: *Ore Geology Reviews*, 39, 21–45. Doi: [10.1016/j.oregeorev.2010.09.002](https://doi.org/10.1016/j.oregeorev.2010.09.002)
- Irvin, T.N., and Baragar, W.R.A., 1971, A guide to chemical classification of the common volcanic rocks: *Canadian Journal Science*, 8, 523–548
- Kamgang, P., Chazot, G., Njonfang, E., Ngongang Tchimegnie, N.B., and Tchoua, F., 2013, Mantle sources and magma evolution beneath the Cameroon volcanic line: geochemistry of mafic rocks from the Bamenda Mountains (NW Cameroon): *Gondwana Research*, 24, 727–741. Doi: [10.1016/j.gr.2012.11.009](https://doi.org/10.1016/j.gr.2012.11.009)
- Kanarian, A., Sarjoughian, F., Nadimi, A., Ahmadian, J., and Ling, W., 2014, Geochemical characteristics of the Kuh-e-Dom intrusion, Urumieh-Dokhtar Magmatic Arc (Iran): implication for source regions and magmatic evolution: *Journal of Asian Earth Sciences*, 90, 137–148. Doi: [10.1016/j.jseaes.2014.04.026](https://doi.org/10.1016/j.jseaes.2014.04.026)
- Kay, S.M., Ramos, V.A., and Marquez, M., 1993, Evidence in Cerro Pampa volcanic rocks of slab melting prior to ridge trench collision in southern South America: *The Journal of Geology*, 101, 703–714. Doi: [10.1086/648269](https://doi.org/10.1086/648269)
- Kebede, T., and Koeberl, C., 2003, Petrogenesis of A-Type granitoids from the Wallagga area, western Ethiopia: constraints from mineralogy, Bulk-rock chemistry, Nd and Sr isotopic compositions: *Precambrian Research*, 121, 1–24. Doi: [10.1016/S0301-9268\(02\)00198-5](https://doi.org/10.1016/S0301-9268(02)00198-5)
- Leake, B.E., Woolley, A.R., Arps, C.E.S., Birch, W.D., Gilbert, M.C., Grice, J.D., Hawthorne, F.C., Kato, A., Kisch, H.J., Krivovichev, V. G., Linthout, K., Laird, J., Mandarino, J., Maresch, W.V., Nickel, E. H., Rock, N.M.S., Schumacher, J.C., Smith, D.C., Stephenson, N.C. N., Ungaretti, L., Whittaker, E.J.W., and Youzhi, G., 1997, Nomenclature of amphiboles: report of the subcommittee on amphiboles of the International Mineralogical Association, commission on new minerals and mineral names: *The Canadian Mineralogist*, 35, 219–246
- Leake, B.F., 1990, Granite magmas, their sources, initiation and consequences of emplacement: *Journal of the Geological Society of London*, 147, 579–589. Doi: [10.1144/gsjgs.147.4.0579](https://doi.org/10.1144/gsjgs.147.4.0579)
- Lemaitre, R.W., Streckeisen, A., Zanettin, B., Le Bas, M.J., Bonin, B., Bateman, P., Bellieni, G., Dudel, A., Efremova, S., Keller, A.J., Lameyre, J., Sabine, P.A., Schmid, R., Sørensen, H., and Woolley, A.R., Eds., 2002, *Igneous Rocks: a Classification and Glossary of Terms: 2nd*, Cambridge, Cambridge University Press, 236
- Liu, Y.S., Gao, S., Hu, Z.C., Gao, C.G., Zong, K.Q., and Wang, D.B., 2010a, Continental and oceanic crust recycling-induced melt-peridotite interactions in the Trans-North China orogeny: U-Pb dating, Hf isotopes and trace elements in zircons of mantle xenoliths: *Journal of Petrology*, 51, 537–571. Doi: [10.1093/petrology/egp082](https://doi.org/10.1093/petrology/egp082)

- Liu, Y.S., Hu, Z.C., Gao, S., Gunther, D., Xu, J., Gao, C.G., and Chen, H.H., 2008, In situ analysis of major and trace elements of anhydrous minerals by LA-ICP-MS without applying an internal standard: *Chemical Geology*, 257, 34–43. Doi: [10.1016/j.chemgeo.2008.08.004](https://doi.org/10.1016/j.chemgeo.2008.08.004)
- Liu, Y.S., Hu, Z.C., Zong, K.Q., Gao, C.G., Gao, S., Xu, J., and Chen, H.H., 2010b, Reappraisal and refinement of zircon U-Pb isotope and trace element analyses by LA-ICP-MS: *Chinese Science Bulletin*, 55, 1535–1546. Doi: [10.1007/s11434-010-3052-4](https://doi.org/10.1007/s11434-010-3052-4)
- Maas, R., Kinny, P.D., Williams, I.S., Froude, D.O., and Compston, W., 1992, The Earth's oldest known crust: a geochronological and geochemical study of 3900–4200 Ma old detrital zircons from Mt. Narryer and Jack Hills, Western Australia: *Geochimica et Cosmochimica Acta*, 56, 1281–1300. Doi: [10.1016/0016-7037\(92\)90062-N](https://doi.org/10.1016/0016-7037(92)90062-N)
- Maniar, P.D., and Piccoli, P.M., 1989, Tectonic discrimination of granitoids: *The Geological Society of America Bulletin*, 101, 635–643. Doi: [10.1130/0016-7606\(1989\)101<0635:TDOG>2.3.CO;2](https://doi.org/10.1130/0016-7606(1989)101<0635:TDOG>2.3.CO;2)
- Mazhari, S.A., Amini, S., Ghalamghash, J., and Bea, F., 2011, Petrogenesis of granitic unit of naqadeh complex, Sanandaj-Sirjan zone, NW Iran: *Arabian Journal of Geosciences*, 4, 59–67. Doi: [10.1007/s12517-009-0077-6](https://doi.org/10.1007/s12517-009-0077-6)
- McDonough, W.F., Sun, S.S., Ringwood, A.E., Jagoutz, E., and Hofmann, A.W., 1992, K, Rb and Cs in the earth and moon and the evolution of the earth's mantle: *Geochimica et Cosmochimica Acta*, 56, 1001–1012. Doi: [10.1016/0016-7037\(92\)90043-I](https://doi.org/10.1016/0016-7037(92)90043-I)
- McInnes, B.I.A., Evans, N.J., Belousova, E., and Griffin, W.L., 2003, Porphyry copper deposits of the Kerman belt, Iran: timing of mineralization and exhumation processes: *Commonwealth Scientific and Industrial Research Organisation Scientific Research*, 77, 1197–1200
- McInnes, B.I.A., Evans, N.J., Fu, F.Q., and Garwin, S., 2005, Application of thermochronology to hydrothermal ore deposits: *Review in Mineralogy and Geochemistry*, 58, 467–498. Doi: [10.2138/rmg.2005.58.18](https://doi.org/10.2138/rmg.2005.58.18)
- Middlemost, E.A.K., 1994, Naming materials in the magma/igneous rock system: *Journal of Earth Science Review*, 37, 215–224. Doi: [10.1016/0012-8252\(94\)90029-9](https://doi.org/10.1016/0012-8252(94)90029-9)
- Miller, C., McDowell, S., and Mapes, R., 2003, Hot and cold granites? Implications of zircon saturation temperatures and preservation of inheritance: *Geology*, 31(6), 529–532. Doi: [10.1130/0091-7613\(2003\)031<0529:HACGIO>2.0.CO;2](https://doi.org/10.1130/0091-7613(2003)031<0529:HACGIO>2.0.CO;2)
- Mohajjel, M., and Fergusson, C., 2000, Dextral transpression in Late Cretaceous continental collision zone. Western Iran: *Journal of Structural Geology*, 22, 1125–1139. Doi: [10.1016/S0191-8141\(00\)00023-7](https://doi.org/10.1016/S0191-8141(00)00023-7)
- Mohajjel, M., Fergusson, C., and Sahandi, M.R., 2003, Cretaceous-Tertiary convergence and continental collision, Sanandaj-Sirjan zone, western Iran: *Journal of Asian Earth Sciences*, 21, 397–412. Doi: [10.1016/S1367-9120\(02\)00035-4](https://doi.org/10.1016/S1367-9120(02)00035-4)
- Morata, D., Oliva, C., de la Cruz, R., and Suarez, M., 2005, The Bandurrias gabbro; late Oligocene alkaline magmatism in the Patagonian cordillera: *Journal of South American Earth Sciences*, 18, 147–162. Doi: [10.1016/j.jsames.2004.09.001](https://doi.org/10.1016/j.jsames.2004.09.001)
- Mouthereau, F., Lacombe, O., and Verges, J., 2012, Building the Zagros collisional orogeny: timing, strain distribution and the dynamics of Arabia/Eurasia plate convergence: *Tectonophysics*, 532, 27–60. Doi: [10.1016/j.tecto.2012.01.022](https://doi.org/10.1016/j.tecto.2012.01.022)
- Muir, R.J., Weaver, S.D., Bradshaw, J.D., Eby, G.N., and Evans, J. A., 1995, Geochemistry of the Cretaceous separation Point batholith, New Zealand: granitoid magmas formed by melting of mafic lithosphere: *Journal of the Geological Society of London*, 152, 689–701. Doi: [10.1144/gsjgs.152.4.0689](https://doi.org/10.1144/gsjgs.152.4.0689)
- Muller, D., 1995, Potassic igneous rocks and associated gold-copper mineralization: *Lecture Notes in Earth Sciences*, 56, 210
- Omran, J., Agard, P., Whitechurch, H., Benoit, M., Prouteau, G., and Jolivet, L., 2008, Arc magmatism and subduction history beneath the Zagros Mountains, Iran: a new report of adakites and geodynamic consequences: *Lithos*, 106, 380–398. Doi: [10.1016/j.lithos.2008.09.008](https://doi.org/10.1016/j.lithos.2008.09.008)
- Patino Douce, A.E., 1999, What do experiments tell us about the relative contributions of crust and mantle to the origin of granitic magmas: *geological society: London, Special Publications*, Vol. 168, 55–75
- Pearce, J.A., Harris, N.B.W., and Tindle, A.G., 1984, Trace element discrimination diagrams for the tectonic interpretation of granitic rocks: *Journal of Petrology*, 25, 956–983. Doi: [10.1093/petrology/25.4.956](https://doi.org/10.1093/petrology/25.4.956)
- Petford, N., and Atherton, M., 1996, Na-rich partial melting's from newly underplated basaltic crust: The Cordillera Blanca batholith, Peru: *Journal of Petrology*, 37, 1491–1521. Doi: [10.1093/petrology/37.6.1491](https://doi.org/10.1093/petrology/37.6.1491)
- Qi, L., Hu, J., and Gregoire, D.C., 2000, Determination of rare elements in granites by inductively coupled plasma mass spectrometry: *Talanta*, 51, 507–513
- Rapp, R.P., and Watson, E.B., 1995, Dehydration melting of metabasalt at 8–32 kbar: implications for continental growth and crust-mantle recycling: *Journal of Petrology*, 36, 891–931. Doi: [10.1093/petrology/36.4.891](https://doi.org/10.1093/petrology/36.4.891)
- Rubatto, D., 2002, Zircon trace element geochemistry: partitioning with garnet and the link between U-Pb ages and metamorphism: *Chemical Geology*, 184, 123–138. Doi: [10.1016/S0009-2541\(01\)00355-2](https://doi.org/10.1016/S0009-2541(01)00355-2)
- Rudnick, R.L., and Fountain, D.M., 1995, Nature and composition of the continental crust: a lower crustal perspective: *Reviews of Geophysics*, 33, 267–309
- Sajona, F.G., Naur, R.C., Pubellier, M., Leterrier, J., Bellon, H., and Cotton, J., 2000, Magmatic source enrichment by slab-derived melts in a young post-collision setting, central Mindanao (Philippines): *Lithos*, 54, 173–206. Doi: [10.1016/S0024-4937\(00\)00019-0](https://doi.org/10.1016/S0024-4937(00)00019-0)
- Saric, V., and Mijalkovic, N., 1973, Kerman metallogenic map: Iran Geological Survey, scale 1:50 000, 1 sheet
- Shafaii Moghadam, H.S., Khademi, M., Hu, Z., Stern, R.J., Santos, J.F., and Wu, Y., 2015, Cadomian (Ediacaran-Cambrian) arc magmatism in the ChahJam-Biarjmand metamorphic complex (Iran): magmatism along the northern active margin of Gondwana: *Gondwana Research*, 27, 439–452. Doi: [10.1016/j.gr.2013.10.014](https://doi.org/10.1016/j.gr.2013.10.014)
- Shafiei, B., 2008, The metallogenic modeling for Kerman porphyry copper belt and implications for exploration [Unpublished PhD thesis], Shahid Bahonar University of Kerman, 311p.
- Shafiei, B., Haschke, M., and Shahabpour, J., 2009, Recycling of orogenic arc crust triggers porphyry Cu mineralization in Kerman Cenozoic arc rocks, southeastern Iran: *Mineralium Deposita*, 44, 265–283. Doi: [10.1007/s00126-008-0216-0](https://doi.org/10.1007/s00126-008-0216-0)

- Shahbapour, J., 2005, Tectonic evolution of the orogenic belt in the region located between Kerman and Neyriz: *Journal of Asian Earth Sciences*, 24, 405–417. Doi: [10.1016/j.jseas.2003.11.007](https://doi.org/10.1016/j.jseas.2003.11.007)
- Shahbapour, J., and Kramers, J.D., 1987, Lead isotope data from the Sar Cheshmeh porphyry copper deposit, Kerman, Iran: *Mineralium Deposita*, 22, 278–281. Doi: [10.1007/BF00204520](https://doi.org/10.1007/BF00204520)
- Shahbazi, H., Siebel, W., Pourmoafae, M., Ghorbani, M., Sepahi, A.A., Shang, C.K., and Vousoughi Abedini, M., 2010, Geochemistry and U-Pb zircon geochronology of the Alvand plutonic complex in Sanandaj-Sirjan Zone (Iran): new evidence for Jurassic magmatism: *Journal of Asian Earth Science*, 39, 668–683. Doi: [10.1016/j.jseas.2010.04.014](https://doi.org/10.1016/j.jseas.2010.04.014)
- Stampfli, G.M., and Borel, G., 2002, A plate tectonic model for the Paleozoic and Mesozoic constrained by dynamic plate boundaries and restored synthetic oceanic isochrones: *Earth and Planetary Science Letters*, 196, 17–33. Doi: [10.1016/S0012-821X\(01\)00588-X](https://doi.org/10.1016/S0012-821X(01)00588-X)
- Stöcklin, J., 1968, Structural history and tectonics of Iran; a review: *Bulletin of the American Association of Petroleum Geologists*, 52, 1229–1258
- Stöcklin, J., and Nabavi, M.H., 1973, Iran tectonic map: Iran Geological Survey, scale 1:250 000, 1 sheet
- Sun, S.S., and McDonough, W.F., 1989, Chemical and isotopic systematics of oceanic basalts: implications for mantle composition and processes, in Saunders, A.D., and Norry, M.J., eds., *Magmatism in the ocean basins*: Geological Society of London Special Publications, 42, 313–345. Doi: [10.1144/gsl.sp.1989.042.01.19](https://doi.org/10.1144/gsl.sp.1989.042.01.19)
- Takin, M., 1972, Iranian geology and continental drift in the Middle East: *Nature*, 235, 147–150. Doi: [10.1038/235147a0](https://doi.org/10.1038/235147a0)
- Taylor, S.R., and McLennan, S., 1985, The continental crust: its composition and evolution: an examination of the geochemical record preserved in sedimentary rocks: *Blackwell Scientific*, 21, 85–86
- Vavra, G., Gebauer, D., Schmid, R., and Compston, W., 1996, Multiple zircon growth and recrystallization during poly phase late Carboniferous to Triassic metamorphism in granulites of the Ivrea Zone (Southern Alps): an ion microprobe (SHRIMP) study: *Contributions to Mineralogy and Petrology*, 122, 337–358. Doi: [10.1007/s004100050132](https://doi.org/10.1007/s004100050132)
- Vavra, G., Schmid, R., and Gebauer, D., 1999, Internal morphology, habit and U-Th-Pb microanalysis of amphibolite to granulite facies zircons: geochronology of the Ivrea Zone (Southern Alps): *Contributions to Mineralogy and Petrology*, 134, 380–404. Doi: [10.1007/s004100050492](https://doi.org/10.1007/s004100050492)
- Verdel, C., Wernicke, B.P., Hassanzadeh, J., and Guest, B., 2011, A paleogene extensional arc flare-up in Iran: *Tectonic*, 30, 3008–3302. Doi: [10.1029/2010TC002809](https://doi.org/10.1029/2010TC002809)
- Wang, Q., Wyman, D.A., Xu, J.F., Zhao, Z.H., Jian, P., Xiong, X.L., Bao, Z.W., Li, C.F., and Bai, Z.H., 2006, Petrogenesis of cretaceous adakitic and shoshonitic igneous rocks in the Luzong area, Anhui Province (eastern China): implications for geodynamics and Cu–Au mineralization: *Lithos*, 89, 424–446. Doi: [10.1016/j.lithos.2005.12.010](https://doi.org/10.1016/j.lithos.2005.12.010)
- Watson, E.B., and Harrison, T.M., 1983, Zircon saturation revised: temperature and composition effects in variety of crustal magma types: *Earth and Planetary Science Letters*, 64, 295–304. Doi: [10.1016/0012-821X\(83\)90211-X](https://doi.org/10.1016/0012-821X(83)90211-X)
- White, A.J.R., and Chappell, B.W., 1983, Granitoid types and their distribution in the Lachlan Fold Belt, southeastern Australia, in Roddick, J.A., ed., *Circum-pacific plutonic terranes*, Vol. 159: *Memoir, Geological Society of America*, 21–34
- Whitney, D.L., and Evans, B.W., 2010, Abbreviations for names of rocks-forming minerals: *American Mineralogist*, 95, 185–187. Doi: [10.2138/am.2010.3371](https://doi.org/10.2138/am.2010.3371)
- Wilson, M., 1989, *Igneous petrogenesis*: Oxford University, Oxford, 466
- Yaganehfar, H., Ghorbani, M.R., Shinjo, R., and Ghaderi, M., 2013, Magmatic and geodynamic evolution of Urumieh-Dokhtar basic volcanism, Central Iran: major, trace element, isotopic, and geochronologic implications: *International Geology Review*, 55, 767–786. Doi: [10.1080/00206814.2012.752554](https://doi.org/10.1080/00206814.2012.752554)
- Zhong, H., Zhu, W.G., Hu, R.Z., Xie, L.W., He, D.F., Liu, F., and Chu, Z.Y., 2009, Zircon U-Pb age and Sr-Nd-Hf isotope geochemistry of the Panzhihua A-type syenitic intrusion in the Emeishan large igneous province, southwest China and implications for growth of juvenile crust: *Lithos*, 110, 109–128. Doi: [10.1016/j.lithos.2008.12.006](https://doi.org/10.1016/j.lithos.2008.12.006)
- Zhou, X.M., Sun, T., Shen, W.Z., Shu, L.S., and Niu, Y.L., 2006, Petrogenesis of Mesozoic granitoids and volcanic rocks in South China: a response to tectonic evolution: *Episode*, 29, 26–33
- Zindler, A., and Hart, S., 1986, Chemical geodynamics: *Review of Earth and Planetary Sciences*, 14, 493–571. Doi: [10.1146/annurev.ea.14.050186.002425](https://doi.org/10.1146/annurev.ea.14.050186.002425)